J Sci Comput (2017) 71:1094–1134
DOI 10.1007/s10915-016-0333-3

Numerical Methods and Comparison for the Dirac Equation in the Nonrelativistic Limit Regime

Weizhu Bao[1] · Yongyong Cai[2,3] · Xiaowei Jia[1] · Qinglin Tang[4]

Received: 6 June 2016 / Revised: 13 November 2016 / Accepted: 7 December 2016 /
Published online: 18 January 2017

Abstract We analyze rigorously error estimates and compare numerically spatial/temporal resolution of various numerical methods for the discretization of the Dirac equation in the nonrelativistic limit regime, involving a small dimensionless parameter $0 < \varepsilon \ll 1$ which is inversely proportional to the speed of light. In this limit regime, the solution is highly oscillatory in time, i.e. there are propagating waves with wavelength $O(\varepsilon^2)$ and $O(1)$ in time and space, respectively. We begin with several frequently used finite difference time domain (FDTD) methods and obtain rigorously their error estimates in the nonrelativistic limit regime by paying particular attention to how error bounds depend explicitly on mesh size h and time step τ as well as the small parameter ε. Based on the error bounds, in order to obtain 'correct' numerical solutions in the nonrelativistic limit regime, i.e. $0 < \varepsilon \ll 1$, the

This work was partially supported by the Ministry of Education of Singapore Grant R-146-000-223-112 (W. Bao and X. Jia), the Natural Science Foundation of China Grant U1530401 and the NSF Grants DMS-1217066 and DMS-1419053 (Y. Cai), and the ANR project BECASIM ANR-12-MONU-0007-02 (Q. Tang).

✉ Yongyong Cai
yongoyng.cai@csrc.ac.cn

Weizhu Bao
matbaowz@nus.edu.sg
http://www.math.nus.edu.sg/∼bao/

Xiaowei Jia
A0068124@nus.edu.sg

Qinglin Tang
tqltql2010@gmail.com

1 Department of Mathematics, National University of Singapore, Singapore 119076, Singapore

2 Beijing Computational Science Research Center, No. 10 West Dongbeiwang Road, Haidian District, Beijing 100193, People's Republic of China

3 Department of Mathematics, Purdue University, West Lafayette, IN 47907, USA

4 Institut Elie Cartan de Lorraine, Inria Nancy-Grand Est, Université de Lorraine, 54506 Vandoeuvre-lès-nancy Cedex, France

FDTD methods share the same ε-scalability on time step and mesh size as: $\tau = O(\varepsilon^3)$ and $h = O(\sqrt{\varepsilon})$. Then we propose and analyze two numerical methods for the discretization of the Dirac equation by using the Fourier spectral discretization for spatial derivatives combined with the symmetric exponential wave integrator and time-splitting technique for temporal derivatives, respectively. Rigorous error bounds for the two numerical methods show that their ε-scalability is improved to $\tau = O(\varepsilon^2)$ and $h = O(1)$ when $0 < \varepsilon \ll 1$. Extensive numerical results are reported to support our error estimates.

Keywords Dirac equation · Nonrelativistic limit regime · Finite difference time domain method · Symmetric exponential wave integrator · Time splitting · Spectral method · ε-Scalability

1 Introduction

The Dirac equation, which plays an important role in particle physics, is a relativistic wave equation derived by the British physicist Paul Dirac in 1928 [28–30,74]. It provided a description of elementary spin-1/2 massive particles, such as electrons and positrons, consistent with both the principle of quantum mechanics and the theory of special relativity. It was the first theory to fully account for relativity in the context of quantum mechanics. It addressed the fine details of the hydrogen spectrum in a completely rigorous way and predicted the existence of a new form of matter, antimatter [4]. Since the graphene was first produced in the lab in 2003 [1,63–65,67], the Dirac equation has been extensively adopted to study theoretically the structures and/or dynamical properties of graphene and graphite as well as two dimensional (2D) materials [62]. This experimental advance renewed extensively the research interests on the mathematical analysis and numerical simulations of the Dirac equation and/or the (nonlinear) Schrödinger equation without/with external potentials, especially the honeycomb lattice potential [3,35].

We consider the three dimensional (3D) Dirac equation for describing the time evolution of spin-1/2 massive particles, such as electrons and positrons, within external time-dependent electromagnetic potentials [28,29]

$$i\hbar\partial_t\Psi = \left[-ic\hbar\sum_{j=1}^{3}\alpha_j\partial_j + mc^2\beta\right]\Psi + e\left[V(t,\mathbf{x})I_4 - \sum_{j=1}^{3}A_j(t,\mathbf{x})\alpha_j\right]\Psi. \tag{1.1}$$

Here, $i = \sqrt{-1}$, t is time, $\mathbf{x} = (x_1, x_2, x_3)^T \in \mathbb{R}^3$ (equivalently written as $\mathbf{x} = (x, y, z)^T$) is the spatial coordinate vector, $\partial_k = \frac{\partial}{\partial x_k}$ $(k = 1, 2, 3)$, $\Psi := \Psi(t, \mathbf{x}) = (\psi_1(t, \mathbf{x}), \psi_2(t, \mathbf{x}), \psi_3(t, \mathbf{x}), \psi_4(t, \mathbf{x}))^T \in \mathbb{C}^4$ is the complex-valued vector wave function of the "spinorfield". I_n is the $n \times n$ identity matrix for $n \in \mathbb{N}$, $V := V(t, \mathbf{x})$ is the real-valued electrical potential and $\mathbf{A} := \mathbf{A}(t, \mathbf{x}) = (A_1(t, \mathbf{x}), A_2(t, \mathbf{x}), A_3(t, \mathbf{x}))^T$ is the real-valued magnetic potential vector, and hence the electric field is given by $\mathbf{E}(t, \mathbf{x}) = -\nabla V - \partial_t\mathbf{A}$ and the magnetic field is given by $\mathbf{B}(t, \mathbf{x}) = \text{curl}\,\mathbf{A} = \nabla \times \mathbf{A}$. The physical constants are: c for the speed of light, m for the particle's rest mass, $\hbar$ for the Planck constant and e for the unit charge. In addition, the 4×4 matrices α_1, α_2, α_3 and β are defined as

$$\alpha_1 = \begin{pmatrix} \mathbf{0} & \sigma_1 \\ \sigma_1 & \mathbf{0} \end{pmatrix}, \quad \alpha_2 = \begin{pmatrix} \mathbf{0} & \sigma_2 \\ \sigma_2 & \mathbf{0} \end{pmatrix}, \quad \alpha_3 = \begin{pmatrix} \mathbf{0} & \sigma_3 \\ \sigma_3 & \mathbf{0} \end{pmatrix}, \quad \beta = \begin{pmatrix} I_2 & \mathbf{0} \\ \mathbf{0} & -I_2 \end{pmatrix}, \tag{1.2}$$

with $\sigma_1, \sigma_2, \sigma_3$ (equivalently written $\sigma_x, \sigma_y, \sigma_z$) being the Pauli matrices defined as

$$\sigma_1 = \begin{pmatrix} 0 & 1 \\ 1 & 0 \end{pmatrix}, \quad \sigma_2 = \begin{pmatrix} 0 & -i \\ i & 0 \end{pmatrix}, \quad \sigma_3 = \begin{pmatrix} 1 & 0 \\ 0 & -1 \end{pmatrix}. \tag{1.3}$$

In order to scale the Dirac equation (1.1), we introduce

$$\tilde{t} = \frac{t}{t_s}, \ \tilde{\mathbf{x}} = \frac{\mathbf{x}}{x_s}, \ \tilde{\Psi}(\tilde{t}, \tilde{\mathbf{x}}) = x_s^{3/2} \Psi(t, \mathbf{x}), \ \tilde{V}(\tilde{t}, \tilde{\mathbf{x}}) = \frac{V(t, \mathbf{x})}{A_s}, \ \tilde{A}_j(\tilde{t}, \tilde{\mathbf{x}}) = \frac{A_j(t, \mathbf{x})}{A_s}, \tag{1.4}$$

where $j = 1, 2, 3$, and x_s, t_s and A_s are the dimensionless length unit, time unit and potential unit, respectively, satisfying $t_s = \frac{m x_s^2}{\hbar}$ and $A_s = \frac{m v^2}{e}$ with $v = \frac{x_s}{t_s}$ being the wave speed. Plugging (1.4) into (1.1), multiplying by $\frac{t_s x_s^{3/2}}{\hbar}$, and then removing all $\tilde{}$, we obtain the following dimensionless Dirac equation in 3D

$$i \partial_t \Psi = \left[-\frac{i}{\varepsilon} \sum_{j=1}^{3} \alpha_j \partial_j + \frac{1}{\varepsilon^2} \beta \right] \Psi + \left[V(t, \mathbf{x}) I_4 - \sum_{j=1}^{3} A_j(t, \mathbf{x}) \alpha_j \right] \Psi, \tag{1.5}$$

where $\mathbf{x} \in \mathbb{R}^3$, and ε is a dimensionless parameter inversely proportional to the speed of light given by

$$0 < \varepsilon := \frac{x_s}{t_s c} = \frac{v}{c} \leq 1. \tag{1.6}$$

We remark here that if one chooses the dimensionless length unit $x_s = \frac{\hbar}{mc}$, $t_s = \frac{x_s}{c}$ and $A_s = \frac{mc^2}{e}$ in (1.4), then $\varepsilon = 1$ in (1.6) and Eq. (1.5) with $\varepsilon = 1$ takes the form often appearing in the literature [2,17,21,23,33,41,49,53]. This choice of x_s is appropriate when the wave speed is at the same order of the speed of light. However, when the wave speed is much smaller than the speed of light, a different choice of x_s is more appropriate. Note that the choice of x_s determines the observation scale of the time evolution of the particles and decides: (i) which phenomena are 'visible' by asymptotic analysis, and (ii) which phenomena can be resolved by discretization by specified spatial/temporal grids. In fact, there are two important parameter regimes: One is $\varepsilon = 1$ ($\Longleftrightarrow x_s = \frac{\hbar}{mc}$, $t_s = \frac{x_s}{c}$ and $A_s = \frac{mc^2}{e}$), then Eq. (1.5) describes the case that wave speed is at the same order of the speed of light; the other one is $0 < \varepsilon \ll 1$, then Eq. (1.5) is in the nonrelativistic limit regime.

Similarly to the dimension reduction of the nonlinear Schrödinger equation and/or the Schrödinger–Poisson equations with/without anisotropic external potentials [8], when the initial data $\Psi(0, \mathbf{x})$ and the electromagnetic potentials $V(t, \mathbf{x})$ and $\mathbf{A}(t, \mathbf{x})$ are independent of z and thus the wave function Ψ is formally assumed to be independent of z, or when the electromagnetic potentials $V(t, \mathbf{x})$ and $\mathbf{A}(t, \mathbf{x})$ are strongly confined in the z-direction and thus Ψ is formally assumed to be concentrated on the xy-plane, then the 3D Dirac equation (1.5) can be reduced to the Dirac equation in 2D with $\mathbf{x} = (x, y)^T \in \mathbb{R}^2$ as

$$i \partial_t \Psi = \left[-\frac{i}{\varepsilon} \sum_{j=1}^{2} \alpha_j \partial_j + \frac{1}{\varepsilon^2} \beta \right] \Psi + \left[V(t, \mathbf{x}) I_4 - \sum_{j=1}^{2} A_j(t, \mathbf{x}) \alpha_j \right] \Psi. \tag{1.7}$$

This 2D Dirac equation has been widely used to model the electron structure and/or dynamical properties of graphene since they share the same dispersion relation on the Dirac points [1,35–37,63–65,67]. Similarly, under the proper assumptions on the initial data and the external electromagnetic potential, the 3D Dirac equation (1.5) can be reduced to the Dirac equation

in 1D with $\Psi = \Psi(t, x)$ as

$$i\partial_t \Psi(t,x) = \left[-\frac{i}{\varepsilon}\alpha_1\partial_x + \frac{1}{\varepsilon^2}\beta\right]\Psi(t,x) + [V(t,x)I_4 - A_1(t,x)\alpha_1]\,\Psi(t,x), \quad x \in \mathbb{R}. \tag{1.8}$$

In fact, the Dirac equation in 3D (1.5), in 2D (1.7) and in 1D (1.8) can be written in a unified way in d-dimensions ($d = 1, 2, 3$)

$$i\partial_t \Psi = \left[-\frac{i}{\varepsilon}\sum_{j=1}^{d}\alpha_j\partial_j + \frac{1}{\varepsilon^2}\beta\right]\Psi + \left[V(t,\mathbf{x})I_4 - \sum_{j=1}^{d}A_j(t,\mathbf{x})\alpha_j\right]\Psi, \tag{1.9}$$

where $\mathbf{x} \in \mathbb{R}^d$ and the initial condition for dynamics is given as

$$\Psi(t=0,\mathbf{x}) = \Psi_0(\mathbf{x}), \quad \mathbf{x} \in \mathbb{R}^d. \tag{1.10}$$

The Dirac equation (1.9) is dispersive and time symmetric. Introducing the position density ρ_j for the j-component ($j = 1, 2, 3, 4$) and the total density ρ as well as the current density $\mathbf{J}(t,\mathbf{x}) = (J_1(t,\mathbf{x}), J_2(t,\mathbf{x}), J_3(t,\mathbf{x}))^T$ for $j = 1, 2, 3, 4$ and $l = 1, 2, 3$

$$\rho(t,\mathbf{x}) = \sum_{j=1}^{4}\rho_j(t,\mathbf{x}) = \Psi^*\Psi, \quad \rho_j(t,\mathbf{x}) = |\psi_j(t,\mathbf{x})|^2; \;\; J_l(t,\mathbf{x}) = \frac{1}{\varepsilon}\Psi^*\alpha_l\Psi, \tag{1.11}$$

where $\overline{f}$ denotes the complex conjugate of f and $\Psi^* = \overline{\Psi}^T$, then the following conservation law can be obtained from the Dirac equation (1.9)

$$\partial_t\rho(t,\mathbf{x}) + \nabla\cdot\mathbf{J}(t,\mathbf{x}) = 0, \quad \mathbf{x} \in \mathbb{R}^d, \quad t \geq 0. \tag{1.12}$$

Thus the Dirac equation (1.9) conserves the total mass as

$$\begin{aligned}\|\Psi(t,\cdot)\|^2 &:= \int_{\mathbb{R}^d}|\Psi(t,\mathbf{x})|^2\,d\mathbf{x} = \int_{\mathbb{R}^d}\sum_{j=1}^{4}|\psi_j(t,\mathbf{x})|^2\,d\mathbf{x}\\ &\equiv \|\Psi(0,\cdot)\|^2 = \|\Psi_0\|^2, \quad t \geq 0.\end{aligned} \tag{1.13}$$

If the electric potential V is perturbed by a real constant V^0, e.g. $V(t,\mathbf{x}) \to V(t,\mathbf{x}) + V^0$, then the solution $\Psi(t,\mathbf{x}) \to e^{-iV^0t}\Psi(t,\mathbf{x})$ which implies the density of each component ρ_j ($j = 1, 2, 3, 4$) and the total density ρ unchanged. When $d = 1$, if the magnetic potential A_1 is perturbed by a real constant A_1^0, e.g. $A_1(t,\mathbf{x}) \to A_1(t,\mathbf{x}) + A_1^0$, then the solution $\Psi(t,\mathbf{x}) \to e^{iA_1^0t\alpha_1}\Psi(t,\mathbf{x})$ which implies the total density ρ unchanged; but this property is not valid when $d = 2, 3$. In addition, when the electromagnetic potentials are time-independent, i.e. $V(t,\mathbf{x}) = V(\mathbf{x})$ and $A_j(t,\mathbf{x}) = A_j(\mathbf{x})$ for $j = 1, 2, 3$, the following energy functional is also conserved

$$\begin{aligned}E(t) &:= \int_{\mathbb{R}^d}\left(-\frac{i}{\varepsilon}\sum_{j=1}^{d}\Psi^*\alpha_j\partial_j\Psi + \frac{1}{\varepsilon^2}\Psi^*\beta\Psi + V(\mathbf{x})|\Psi|^2 - \sum_{j=1}^{d}A_j(\mathbf{x})\Psi^*\alpha_j\Psi\right)d\mathbf{x}\\ &\equiv E(0), \quad t \geq 0.\end{aligned} \tag{1.14}$$

Furthermore, if the external electromagnetic potentials are constants, i.e. $V(t,\mathbf{x}) \equiv V^0$ and $A_j(t,\mathbf{x}) \equiv A_j^0$ for $j = 1, 2, 3$ with $\mathbf{A}^0 = (A_1^0, \ldots, A_d^0)^T$, the Dirac equation (1.9) admits the plane wave solution as $\Psi(t,\mathbf{x}) = \mathbf{B}\,e^{i(\mathbf{k}\cdot\mathbf{x}-\omega t)}$, where the time frequency ω, amplitude vector

$\mathbf{B} \in \mathbb{R}^4$ and spatial wave number $\mathbf{k} = (k_1, \ldots, k_d)^T \in \mathbb{R}^d$ satisfy the following *dispersion relation*

$$\omega \mathbf{B} = \left[\sum_{j=1}^{d} \left(\frac{k_j}{\varepsilon} - A_j^0 \right) \alpha_j + \frac{1}{\varepsilon^2} \beta + V^0 I_4 \right] \mathbf{B}, \tag{1.15}$$

which immediately implies the dispersion relation of the Dirac equation (1.9) as

$$\omega := \omega(\mathbf{k}) = V^0 \pm \frac{1}{\varepsilon^2} \sqrt{1 + \varepsilon^2 \left| \mathbf{k} - \varepsilon \mathbf{A}^0 \right|^2} = O\left(\frac{1}{\varepsilon^2} \right), \quad \mathbf{k} \in \mathbb{R}^d. \tag{1.16}$$

Plugging (1.2) and (1.3) into (1.7), the 2D Dirac equation (1.7) can be decoupled for $\mathbf{x} \in \mathbb{R}^2$ as

$$\begin{aligned} i\partial_t \psi_1 &= -\frac{i}{\varepsilon} \left(\partial_x - i\partial_y \right) \psi_4 + \frac{1}{\varepsilon^2} \psi_1 + V(t, \mathbf{x}) \psi_1 - \left[A_1(t, \mathbf{x}) - i A_2(t, \mathbf{x}) \right] \psi_4, \\ i\partial_t \psi_4 &= -\frac{i}{\varepsilon} \left(\partial_x + i\partial_y \right) \psi_1 - \frac{1}{\varepsilon^2} \psi_4 + V(t, \mathbf{x}) \psi_4 - \left[A_1(t, \mathbf{x}) + i A_2(t, \mathbf{x}) \right] \psi_1, \end{aligned} \tag{1.17}$$

$$\begin{aligned} i\partial_t \psi_2 &= -\frac{i}{\varepsilon} \left(\partial_x + i\partial_y \right) \psi_3 + \frac{1}{\varepsilon^2} \psi_2 + V(t, \mathbf{x}) \psi_2 - \left[A_1(t, \mathbf{x}) + i A_2(t, \mathbf{x}) \right] \psi_3, \\ i\partial_t \psi_3 &= -\frac{i}{\varepsilon} \left(\partial_x - i\partial_y \right) \psi_2 - \frac{1}{\varepsilon^2} \psi_3 + V(t, \mathbf{x}) \psi_3 - \left[A_1(t, \mathbf{x}) - i A_2(t, \mathbf{x}) \right] \psi_2. \end{aligned} \tag{1.18}$$

Equation (1.18) will collapse to (1.17) under the transformation $y \to -y$ and $A_2 \to -A_2$. Thus, in 2D, the Dirac equation (1.7) can be reduced to the following simplified PDEs with $\Phi := \Phi(t, \mathbf{x}) = (\phi_1(t, \mathbf{x}), \phi_2(t, \mathbf{x}))^T \in \mathbb{C}^2$

$$i\partial_t \Phi = \left[-\frac{i}{\varepsilon} \left(\sigma_1 \partial_x + \sigma_2 \partial_y \right) + \frac{1}{\varepsilon^2} \sigma_3 \right] \Phi + \left[V(t, \mathbf{x}) I_2 - A_1(t, \mathbf{x}) \sigma_1 - A_2(t, \mathbf{x}) \sigma_2 \right] \Phi, \tag{1.19}$$

where $\Phi = (\psi_1, \psi_4)^T$ (or $\Phi = (\psi_2, \psi_3)^T$ under the transformation $y \to -y$ and $A_2 \to -A_2$). Similarly, in 1D, the Dirac equation (1.8) can be reduced to the following simplified PDEs with $\Phi = \Phi(t, x) = (\phi_1(t, x), \phi_2(t, x))^T$

$$i\partial_t \Phi = \left[-\frac{i}{\varepsilon} \sigma_1 \partial_x + \frac{1}{\varepsilon^2} \sigma_3 \right] \Phi + \left[V(t, x) I_2 - A_1(t, x) \sigma_1 \right] \Phi, \quad x \in \mathbb{R}, \tag{1.20}$$

where $\Phi = (\psi_1, \psi_4)^T$ (or $\Phi = (\psi_2, \psi_3)^T$). Again, the Dirac equation in 2D (1.19) and in 1D (1.20) can be written in a unified way for $\mathbf{x} \in \mathbb{R}^d$ in d-dimensions ($d = 1, 2$)

$$i\partial_t \Phi = \left[-\frac{i}{\varepsilon} \sum_{j=1}^{d} \sigma_j \partial_j + \frac{1}{\varepsilon^2} \sigma_3 \right] \Phi + \left[V(t, \mathbf{x}) I_2 - \sum_{j=1}^{d} A_j(t, \mathbf{x}) \sigma_j \right] \Phi, \tag{1.21}$$

and the initial condition for dynamics is given as

$$\Phi(t = 0, \mathbf{x}) = \Phi_0(\mathbf{x}), \quad \mathbf{x} \in \mathbb{R}^d. \tag{1.22}$$

The Dirac equation (1.21) is dispersive and time symmetric. By introducing the position density ρ_j for the j-th component ($j = 1, 2$) and the total density ρ as well as the current density $\mathbf{J}(t, \mathbf{x}) = (J_1(t, \mathbf{x}), J_2(t, \mathbf{x}))^T$

$$\rho(t, \mathbf{x}) = \sum_{j=1}^{2} \rho_j(t, \mathbf{x}) = \Phi^* \Phi, \ \rho_j(t, \mathbf{x}) = |\phi_j(t, \mathbf{x})|^2, \ J_j(t, \mathbf{x}) = \frac{1}{\varepsilon} \Phi^* \sigma_j \Phi, \quad j = 1, 2, \tag{1.23}$$

the conservation law (1.12) is also satisfied [23]. In addition, the Dirac equation (1.21) conserves the total mass as

$$\|\Phi(t,\cdot)\|^2 := \int_{\mathbb{R}^d} |\Phi(t,\mathbf{x})|^2\, d\mathbf{x} = \int_{\mathbb{R}^d} \sum_{j=1}^{2} |\phi_j(t,\mathbf{x})|^2\, d\mathbf{x}$$
$$\equiv \|\Phi(0,\cdot)\|^2 = \|\Phi_0\|^2, \quad t \geq 0. \tag{1.24}$$

Again, if the electric potential V is perturbed by a real constant V^0, e.g. $V(t,\mathbf{x}) \to V(t,\mathbf{x}) + V^0$, the solution $\Phi(t,\mathbf{x}) \to e^{-iV^0 t}\Phi(t,\mathbf{x})$ which implies the density of each component ρ_j $(j = 1, 2)$ and the total density ρ unchanged. When $d = 1$, if the magnetic potential A_1 is perturbed by a real constant A_1^0, e.g. $A_1(t,\mathbf{x}) \to A_1(t,\mathbf{x}) + A_1^0$, the solution $\Phi(t,\mathbf{x}) \to e^{iA_1^0 t\sigma_1}\Phi(t,\mathbf{x})$ implying the total density ρ unchanged; but this property is not valid when $d = 2$. When the electromagnetic potentials are time-independent, i.e. $V(t,\mathbf{x}) = V(\mathbf{x})$ and $A_j(t,\mathbf{x}) = A_j(\mathbf{x})$ for $j = 1, 2$, the following energy functional is also conserved

$$E(t) := \int_{\mathbb{R}^d} \left(-\frac{i}{\varepsilon} \sum_{j=1}^{d} \Phi^* \sigma_j \partial_j \Phi + \frac{1}{\varepsilon^2} \Phi^* \sigma_3 \Phi + V(\mathbf{x})|\Phi|^2 - \sum_{j=1}^{d} A_j(\mathbf{x}) \Phi^* \sigma_j \Phi \right) d\mathbf{x}$$
$$\equiv E(0), \quad t \geq 0. \tag{1.25}$$

Furthermore, if the external electromagnetic potentials are constants, i.e. $V(t,\mathbf{x}) \equiv V^0$ and $A_j(t,\mathbf{x}) \equiv A_j^0$ for $j = 1, 2$, the Dirac equation (1.21) admits the plane wave solution as $\Phi(t,\mathbf{x}) = \mathbf{B}\, e^{i(\mathbf{k}\cdot\mathbf{x}-\omega t)}$, where the time frequency ω, amplitude vector $\mathbf{B} \in \mathbb{R}^2$ and spatial wave number $\mathbf{k} = (k_1, \ldots, k_d)^T \in \mathbb{R}^d$ satisfy the following *dispersion relation*

$$\omega \mathbf{B} = \left[\sum_{j=1}^{d} \left(\frac{k_j}{\varepsilon} - A_j^0 \right) \sigma_j + \frac{1}{\varepsilon^2} \sigma_3 + V^0 I_2 \right] \mathbf{B}, \tag{1.26}$$

which again implies the dispersion relation (1.16) of the Dirac equation (1.21) for $d = 2, 1$.

For the Dirac equation (1.9) with $\varepsilon = 1$, i.e. $O(1)$-speed of light regime, there are extensive analytical and numerical results in the literatures. For the existence and multiplicity of bound states and/or standing wave solutions, we refer to [25,26,31,32,44,47,75] and references therein. For the analysis of the classical/semiclassical limits via the Wigner transform techniques, we refer to [7,20,22,43,57,72] and references therein. For the numerical methods and comparison such as the finite difference time domain (FDTD) methods and the Gaussian beam methods, we refer to [5,7,27,38,39,45,69,77] and references therein. However, for the Dirac equation (1.9) with $0 < \varepsilon \ll 1$, i.e. nonrelativistic limit regime (or the scaled speed of light goes to infinity), the analysis and efficient computation of the Dirac equation (1.9) (or 1.21) are mathematically rather complicated. The main difficulty is due to that the solution is highly oscillatory in time and the corresponding energy functionals (1.14) and (1.25) are indefinite [18,33] and become unbounded when $\varepsilon \to 0$. There are extensive mathematical analysis of the (semi)-nonrelativistic limit of the Dirac equation (1.9) to the Pauli equation [18,19,24,40,46,54,59–61,68,76] and/or the Schrödinger equation when $\varepsilon \to 0$ [18]. These rigorous analytical results show that the solution propagates waves with wavelength $O(\varepsilon^2)$ and $O(1)$ in time and space, respectively, when $0 < \varepsilon \ll 1$. In fact, the oscillatory structure of the solution of the Dirac equation (1.9) when $0 < \varepsilon \ll 1$ can be formally observed from its dispersion relation (1.15) (or 1.26). To illustrate this further, Fig. 1 shows the solution of the Dirac equation (1.21) with $d = 1$, $V(t,x) = \frac{1-x}{1+x^2}$, $A_1(t,x) = \frac{(1+x)^2}{1+x^2}$

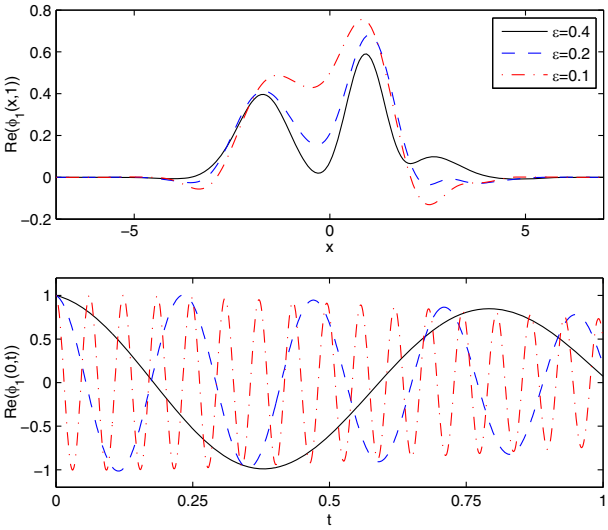

Fig. 1 The solution $\phi_1(t = 1, x)$ and $\phi_1(t, x = 0)$ of the Dirac equation (1.21) with $d = 1$ for different ε. $\mathrm{Re}(f)$ denotes the real part of f

and $\Phi_0(x) = \left(\exp(-x^2/2), \exp(-(x-1)^2/2)\right)^T$ for different ε. This highly oscillatory nature of the solution of (1.9) (or 1.21) causes severe numerical burdens in practical computation, making the numerical approximation of (1.9) (or 1.21) extremely challenging and costly in the nonrelativistic regime $0 < \varepsilon \ll 1$. In [53], the resolution of the time-splitting Fourier pseudospectral (TSFP) method was studied for the Maxwell–Dirac equation in the nonrelativistic limit regime.

Recently, different numerical methods were proposed and analyzed for the efficient computation of the Klein–Gordon equation in the nonrelativistic limit regime [11,12,34] and/or highly oscillatory dispersive partial differential equations (PDEs) [9,10,13,14]. To our knowledge, so far there are few results on the numerics of the Dirac equation in the nonrelativistic limit regime. The aim of this paper is to study the efficiency of the frequently used FDTD and TSFP methods applied to the Dirac equation in the nonrelativistic limit regime, to propose the symmetric exponential wave integrator Fourier pseudospectral (sEWI-FP) method and to compare their resolution capacities in this regime. We start with the detailed analysis on the stability and convergence of several standard implicit/semi-implicit/explicit FDTD methods [71]. Here we pay particular attention to how the error bounds depend explicitly on the small parameter ε in addition to the mesh size h and time step τ. Based on the estimates, in order to obtain 'correct' numerical approximations when $0 < \varepsilon \ll 1$, the meshing strategy requirement (ε-scalability) for those frequently used FDTD methods is: $h = O(\sqrt{\varepsilon})$ and $\tau = O(\varepsilon^3)$, which suggests that the standard FDTD methods are computationally expensive for the Dirac equation (1.9) as $0 < \varepsilon \ll 1$. To relax the ε-scalability, we then propose the sEWI-FP method and compare it with the TSFP method, whose ε-scalability are optimal for both time and space in view of the inherent oscillatory nature. The key ideas of the sEWI-FP are: (i) to apply the Fourier pseudospectral discretization for spatial derivatives; and (ii) to adopt the symmetric exponential wave integrator (sEWI) for integrating the ordinary differential equations (ODEs) in phase space [42,50] which was well demonstrated in the literatures that it has favorable properties compared to standard time integrators for oscilla-

tory differential equations [42,50–52]. Rigorous error estimates show that the ε-scalability of the sEWI-FP method is $h = O(1)$, and $\tau = O(\varepsilon^2)$ for the Dirac equation with external electromagnetic potentials, meanwhile, the ε-scalability of TSFP method is $h = O(1)$ and $\tau = O(\varepsilon^2)$. Thus, the sEWI-FP and TSFP offer compelling advantages over commonly used FDTD methods in temporal and spatial resolution when $0 < \varepsilon \ll 1$.

The rest of this paper is organized as follows. In Sect. 2, several second-order FDTD methods are reviewed and their stabilities and convergence are analyzed in the nonrelativistic limit regime. In Sect. 3, a symmetric exponential wave integrator Fourier pseudospectral method is proposed and analyzed rigorously. In Sect. 4, a time-splitting Fourier pseudospectral method is reviewed and analyzed rigorously. In Sect. 5, numerical comparison results are reported. Finally, some concluding remarks are drawn in Sect. 6. The mathematical proofs of the error estimates are given in the appendices, where extensions of sEWI-FP and TSFP to higher dimensions are also presented. Throughout the paper, we adopt the standard notations of Sobolev spaces, use the notation $p \lesssim q$ to represent that there exists a generic constant C which is independent of h, τ and ε such that $|p| \leq C\, q$.

2 FDTD Methods and Their Analysis

In this section, we apply the commonly used FDTD methods to the Dirac equation (1.9) (or 1.21) and analyze their stabilities and convergence in the nonrelativistic limit regime. For simplicity of notations, we shall only present the numerical methods and their analysis for (1.21) in 1D. Generalization to (1.9) and/or higher dimensions is straightforward and results remain valid without modifications. Similarly to most works in the literatures for the analysis and computation of the Dirac equation (cf. [17,23,48,49,53,66,77] and references therein), in practical computation, we truncate the whole space problem onto an interval $\Omega = (a, b)$ with periodic boundary conditions, which is large enough such that the truncation error is negligible. In 1D, the Dirac equation (1.21) with periodic boundary conditions collapses to

$$i\partial_t \Phi = \left[-\frac{i}{\varepsilon}\sigma_1\partial_x + \frac{1}{\varepsilon^2}\sigma_3\right]\Phi + [V(t,x)I_2 - A_1(t,x)\sigma_1]\,\Phi,\ x \in \Omega,\ t > 0, \tag{2.1}$$

$$\Phi(t,a) = \Phi(t,b),\ \partial_x\Phi(t,a) = \partial_x\Phi(t,b),\ t \geq 0;\ \Phi(0,x) = \Phi_0(x), \quad x \in \overline{\Omega}, \tag{2.2}$$

where $\Phi := \Phi(t,x)$, $\Phi_0(a) = \Phi_0(b)$ and $\Phi_0'(a) = \Phi_0'(b)$.

2.1 FDTD Methods

Choose mesh size $h := \Delta x = \frac{b-a}{M}$ with M being an even positive integer, time step $\tau := \Delta t > 0$ and denote the grid points and time steps as:

$$x_j := a + jh, \quad j = 0, 1, \ldots, M; \quad t_n := n\tau, \quad n = 0, 1, 2, \ldots.$$

Denote $X_M = \{U = (U_0, U_1, \ldots, U_M)^T \mid U_j \in \mathbb{C}^2,\ j = 0, 1, \ldots, M,\ U_0 = U_M\}$ and we always use $U_{-1} = U_{M-1}$ and $U_{M+1} = U_1$ if they are involved. For any $U \in X_M$, we denote its Fourier representation as

$$U_j = \sum_{l=-M/2}^{M/2-1} \widetilde{U}_l\, e^{i\mu_l(x_j-a)} = \sum_{l=-M/2}^{M/2-1} \widetilde{U}_l\, e^{2ijl\pi/M}, \quad j = 0, 1, \ldots, M, \tag{2.3}$$

where μ_l and $\widetilde{U}_l \in \mathbb{C}^2$ are defined as

$$\mu_l = \frac{2l\pi}{b-a}, \quad \widetilde{U}_l = \frac{1}{M}\sum_{j=0}^{M-1} U_j\, e^{-2ijl\pi/M}, \quad l = -\frac{M}{2}, \ldots, \frac{M}{2}-1. \tag{2.4}$$

The standard l^2-norm in X_M is given as

$$\|U\|_{l^2}^2 = h\sum_{j=0}^{M-1} |U_j|^2, \quad U \in X_M. \tag{2.5}$$

Let Φ_j^n be the numerical approximation of $\Phi(t_n, x_j)$ and $V_j^n = V(t_n, x_j)$, $V_j^{n+1/2} = V(t_n + \tau/2, x_j)$, $A_{1,j}^n = A_1(t_n, x_j)$ and $A_{1,j}^{n+1/2} = A_1(t_n + \tau/2, x_j)$ for $0 \le j \le M$ and $n \ge 0$. Denote $\Phi^n = \left(\Phi_0^n, \Phi_1^n, \ldots, \Phi_M^n\right)^T \in X_M$ as the solution vector at $t = t_n$. Introduce the finite difference discretization operators for $j = 0, 1, \ldots, M$ and $n \ge 0$ as:

$$\delta_t^+ \Phi_j^n = \frac{\Phi_j^{n+1} - \Phi_j^n}{\tau}, \quad \delta_t \Phi_j^n = \frac{\Phi_j^{n+1} - \Phi_j^{n-1}}{2\tau}, \quad \delta_x \Phi_j^n = \frac{\Phi_{j+1}^n - \Phi_{j-1}^n}{2h},$$

and the average as

$$\Phi_j^{n+\frac{1}{2}} = \frac{\Phi_j^{n+1} + \Phi_j^n}{2}.$$

Here we consider several frequently used FDTD methods to discretize the Dirac equation (2.1) for $j = 0, 1, \ldots, M-1$.

I. Leap-frog finite difference (LFFD) method, for $n \ge 1$,

$$i\delta_t \Phi_j^n = \left[-\frac{i}{\varepsilon}\sigma_1\delta_x + \frac{1}{\varepsilon^2}\sigma_3\right]\Phi_j^n + \left[V_j^n I_2 - A_{1,j}^n\sigma_1\right]\Phi_j^n. \tag{2.6}$$

II. Semi-implicit finite difference (SIFD1) method, for $n \ge 1$,

$$i\delta_t \Phi_j^n = -\frac{i}{\varepsilon}\sigma_1\delta_x\Phi_j^n + \left[\frac{1}{\varepsilon^2}\sigma_3 + V_j^n I_2 - A_{1,j}^n\sigma_1\right]\frac{\Phi_j^{n+1} + \Phi_j^{n-1}}{2}. \tag{2.7}$$

III. Another semi-implicit finite difference (SIFD2) method, for $n \ge 1$,

$$i\delta_t \Phi_j^n = \left[-\frac{i}{\varepsilon}\sigma_1\delta_x + \frac{1}{\varepsilon^2}\sigma_3\right]\frac{\Phi_j^{n+1} + \Phi_j^{n-1}}{2} + \left[V_j^n I_2 - A_{1,j}^n\sigma_1\right]\Phi_j^n. \tag{2.8}$$

IV. Crank-Nicolson finite difference (CNFD) method, for $n \ge 0$,

$$i\delta_t^+ \Phi_j^n = \left[-\frac{i}{\varepsilon}\sigma_1\delta_x + \frac{1}{\varepsilon^2}\sigma_3\right]\Phi_j^{n+1/2} + \left[V_j^{n+1/2} I_2 - A_{1,j}^{n+1/2}\sigma_1\right]\Phi_j^{n+1/2}. \tag{2.9}$$

The initial and boundary conditions in (2.2) are discretized as:

$$\Phi_M^{n+1} = \Phi_0^{n+1}, \ \Phi_{-1}^{n+1} = \Phi_{M-1}^{n+1}, \ n \ge 0; \quad \Phi_j^0 = \Phi_0(x_j), \ j = 0, 1, \ldots, M. \tag{2.10}$$

Using Taylor expansion and noticing (2.1), the first step for the LFFD (2.6), SIFD1 (2.7) and SIFD2 (2.8) can be computed as

$$\Phi_j^1 = \Phi_j^0 - \sin\left(\frac{\tau}{\varepsilon}\right)\sigma_1\Phi_0'(x_j) - i\left[\sin\left(\frac{\tau}{\varepsilon^2}\right)\sigma_3 + \tau V_j^0 I_2 - \tau A_{1,j}^0\sigma_1\right]\Phi_j^0, \tag{2.11}$$

where $j = 0, 1, \ldots, M$. In the above, we adopt $\frac{1}{\tau}\sin\left(\frac{\tau}{\varepsilon}\right)$ and $\frac{1}{\tau}\sin\left(\frac{\tau}{\varepsilon^2}\right)$ instead of $\frac{1}{\varepsilon}$ and $\frac{1}{\varepsilon^2}$ such that (2.11) is second order in term of τ for any fixed $0 < \varepsilon \leq 1$ and $\|\Phi^1\|_\infty := \max\limits_{0\leq j\leq M} |\Phi_j^1| \lesssim 1$ for $0 < \varepsilon \leq 1$. We remark here that they can be simply replaced by 1 when $\varepsilon = 1$.

The above four methods are all time symmetric, i.e. they are unchanged under $\tau \leftrightarrow -\tau$ and $n+1 \leftrightarrow n-1$ in the LFFD, SIFD1 and SIFD2 methods or $n+1 \leftrightarrow n$ in the CNFD method, and the memory cost is the same at $O(M)$. The LFFD method (2.6) is explicit and its computational cost per step is $O(M)$. In fact, it might be the simplest and most efficient discretization for the Dirac equation when $\varepsilon = 1$ and thus it has been widely used when $\varepsilon = 1$. The SIFD1 method (2.7) is implicit, however at each time step for $n \geq 1$, the corresponding linear system is decoupled and can be solved explicitly for $j = 0, 1, \ldots, M-1$ as

$$\Phi_j^{n+1} = \left[(i - \tau V_j^n) I_2 - \frac{\tau}{\varepsilon^2}\sigma_3 + \tau A_{1,j}^n \sigma_1\right]^{-1} H_j^n,$$

with $H_j^n = \left[\left((i + \tau V_j^n) I_2 + \frac{\tau}{\varepsilon^2}\sigma_3 - \tau A_{1,j}^n \sigma_1\right)\Phi_j^{n-1} - \frac{2i\tau}{\varepsilon}\sigma_1 \delta_x \Phi_j^n\right]$, and thus its computational cost per step is $O(M)$.

The SIFD2 method (2.8) is implicit, however at each time step for $n \geq 1$, the corresponding linear system is decoupled in phase (Fourier) space and can be solved explicitly in phase space for $l = -M/2, \ldots, M/2 - 1$ as

$$\widetilde{(\Phi^{n+1})}_l = \left(i I_2 - \frac{\tau \sin(\mu_l h)}{\varepsilon h}\sigma_1 - \frac{\tau}{\varepsilon^2}\sigma_3\right)^{-1} L_l^n, \tag{2.12}$$

where

$$L_l^n = \left[\left(i I_2 + \frac{\tau \sin(\mu_l h)}{\varepsilon h}\sigma_1 + \frac{\tau}{\varepsilon^2}\sigma_3\right)\widetilde{(\Phi^{n-1})}_l + 2\tau \widetilde{(G^n \Phi^n)}_l\right],$$

and $G^n = (G_0^n, G_1^n, \ldots, G_M^n)^T \in X_M$ with $G_j^n = -A_{1,j}^n \sigma_1 + V_j^n I_2$ for $j = 0, 1, \ldots, M$, and thus its computational cost per step is $O(M \ln M)$. The CNFD method (2.9) is implicit and at each time step for $n \geq 0$, the corresponding linear system is coupled and needs to be solved via either a direct solver or an iterative solver, and thus its computational cost per step depends on the linear system solver, which is usually much larger than $O(M)$, especially in 2D and 3D. Based on the computational cost per time step, the LFFD method is the most efficient one and the CNFD method is the most expensive one.

2.2 Linear Stability Analysis

In order to carry out the linear stability analysis for the FDTD methods via the von Neumann method [71], we assume that $A_1(t, x) \equiv A_1^0$ and $V(t, x) \equiv V^0$ with A_1^0 and V^0 being two real constants in the Dirac equation (2.1). Then we have the following results for the FDTD methods:

Lemma 2.1 (i) *The LFFD method (2.6) is stable under the stability condition*

$$0 < \tau \leq \frac{\varepsilon^2 h}{|V^0|\varepsilon^2 h + \sqrt{h^2 + \varepsilon^2(1 + \varepsilon h |A_1^0|)^2}}, \quad h > 0, \quad 0 < \varepsilon \leq 1. \tag{2.13}$$

(ii) *The SIFD1 method (2.7) is stable under the stability condition*

$$0 < \tau \leq \varepsilon h, \quad h > 0, \quad 0 < \varepsilon \leq 1. \tag{2.14}$$

(iii) *The SIFD2 method (2.8) is stable under the stability condition*

$$0 < \tau \le \frac{1}{|V^0| + |A_1^0|}, \quad h > 0, \quad 0 < \varepsilon \le 1. \tag{2.15}$$

(iv) *The CNFD method (2.9) is unconditionally stable, i.e. it is stable for any* $\tau, h > 0$ *and* $0 < \varepsilon \le 1$.

Proof (i) Plugging

$$\Phi_j^n = \sum_{l=-M/2}^{M/2-1} \xi_l^n \widetilde{(\Phi^0)}_l \, e^{i\mu_l(x_j-a)} = \sum_{l=-M/2}^{M/2-1} \xi_l^n \widetilde{(\Phi^0)}_l \, e^{2ijl\pi/M}, \ 0 \le j \le M, \tag{2.16}$$

with $\xi_l \in \mathbb{C}$ and $\widetilde{(\Phi^0)}_l$ being the amplification factor and the Fourier coefficient at $n = 0$, respectively, of the l-th mode in the phase space into (2.6), using the orthogonality of the Fourier series, we obtain for $l = -\frac{M}{2}, \ldots, \frac{M}{2} - 1$,

$$\left| (\xi_l^2 - 1) I_2 - 2i\tau\xi_l \left(A_1^0\sigma_1 - V^0 I_2 - \frac{1}{\varepsilon^2}\sigma_3 - \frac{\sin(\mu_l h)}{\varepsilon h}\sigma_1 \right) \right| = 0. \tag{2.17}$$

Substituting (1.3) into (2.17), we get that the amplification factor ξ_l satisfies

$$\xi_l^2 - 2i\tau\theta_l\xi_l - 1 = 0, \quad l = -\frac{M}{2}, \ldots, \frac{M}{2} - 1, \tag{2.18}$$

where

$$\theta_l = -V^0 \pm \frac{1}{\varepsilon^2 h}\sqrt{h^2 + \varepsilon^2 \left(A_1^0 \varepsilon h - \sin(\mu_l h) \right)^2}, \quad l = -\frac{M}{2}, \ldots, \frac{M}{2} - 1.$$

Then the stability condition for the LFFD method (2.6) becomes

$$|\xi_l| \le 1 \iff |\tau\theta_l| \le 1, \quad l = -\frac{M}{2}, \ldots, \frac{M}{2} - 1, \tag{2.19}$$

which immediately implies the condition (2.13).

(ii) Similarly to (i), plugging (2.16) into the SIFD1 method (2.7), we have for $l = -\frac{M}{2}, \ldots, \frac{M}{2} - 1$,

$$\left| (\xi_l^2 - 1) I_2 - i\tau(\xi_l^2 + 1) \left(A_1^0\sigma_1 - V^0 I_2 - \frac{1}{\varepsilon^2}\sigma_3 \right) + \frac{2i\tau\xi_l \sin(\mu_l h)}{\varepsilon h}\sigma_1 \right| = 0. \tag{2.20}$$

Noticing (1.3), under the condition (2.14), we can get $|\xi_l| \le 1$ for $l = -\frac{M}{2}, \ldots, \frac{M}{2} - 1$, and thus it is stable.

(iii) Similarly to (i), plugging (2.16) into the SIFD2 method (2.8), we have for $l = -\frac{M}{2}, \ldots, \frac{M}{2} - 1$,

$$\left| (\xi_l^2 - 1) I_2 + i\tau(\xi_l^2 + 1) \left(\frac{1}{\varepsilon^2}\sigma_3 + \frac{\sin(\mu_l h)}{\varepsilon h}\sigma_1 \right) - 2i\tau\xi_l (A_1^0\sigma_1 - V^0 I_2) \right| = 0. \tag{2.21}$$

Noticing (1.3), under the condition (2.15), we obtain

$$|\xi_l| \le 1, \quad l = -\frac{M}{2}, \ldots, \frac{M}{2} - 1,$$

and thus it is stable.

(iv) Similarly to (i), plugging (2.16) into the CNFD method (2.9), we obtain for $l = -\frac{M}{2}, \ldots, \frac{M}{2} - 1$,

$$\left|(\xi_l - 1)I_2 + \frac{i\tau}{2}(\xi_l + 1)\left(\frac{1}{\varepsilon^2}\sigma_3 - A_1^0\sigma_1 - V^0 I_2 + \frac{\sin(\mu_l h)}{\varepsilon h}\sigma_1\right)\right| = 0. \tag{2.22}$$

Noticing (1.3), we have for $l = -\frac{M}{2}, \ldots, \frac{M}{2} - 1$,

$$|\xi_l| = \left|\frac{2 + i\tau\theta_l}{2 - i\tau\theta_l}\right| = 1, \quad \theta_l = V^0 \pm \frac{1}{\varepsilon^2 h}\sqrt{h^2 + \varepsilon^2\left(A_1^0\varepsilon h - \sin(\mu_l h)\right)^2}. \tag{2.23}$$

Thus it is unconditionally stable. □

2.3 Mass and Energy Conservation

For the CNFD method (2.9), we have the following conservative properties.

Lemma 2.2 *The CNFD (2.9) conserves the mass in the discretized level, i.e.*

$$\|\Phi^n\|_{l^2}^2 := h\sum_{j=0}^{M-1}|\Phi_j^n|^2 \equiv h\sum_{j=0}^{M-1}|\Phi_j^0|^2 = \|\Phi^0\|_{l^2}^2 = h\sum_{j=0}^{M-1}|\Phi_0(x_j)|^2,\ n \geq 0. \tag{2.24}$$

Furthermore, if $V(t,x) = V(x)$ and $A_1(t,x) = A_1(x)$ are time independent, the CNFD (2.9) conserves the energy as well,

$$\begin{aligned} E_h^n =& h\sum_{j=0}^{M-1}\left[-\frac{i}{\varepsilon}(\Phi_j^n)^*\sigma_1\delta_x\Phi_j^n + \frac{1}{\varepsilon^2}(\Phi_j^n)^*\sigma_3\Phi_j^n + V_j|\Phi_j^n|^2 - A_{1,j}(\Phi_j^n)^*\sigma_1\Phi_j^n\right] \\ \equiv& E_h^0, \quad n \geq 0, \end{aligned} \tag{2.25}$$

where $V_j = V(x_j)$ and $A_{1,j} = A_1(x_j)$ for $j = 0, 1, \ldots, M$.

Proof (i) Firstly, we prove the mass conservation (2.24). Multiplying both sides of (2.9) from left by $h\tau\,(\Phi_j^{n+1/2})^*$ and taking the imaginary part, we have for $j = 0, 1, \ldots, M-1$,

$$h|\Phi_j^{n+1}|^2 = h|\Phi_j^n|^2 - \frac{\tau h}{2\varepsilon}\left[(\Phi_j^{n+1/2})^*\sigma_1\delta_x\Phi_j^{n+1/2} + (\Phi_j^{n+1/2})^T\sigma_1\delta_x\overline{\Phi}_j^{n+1/2}\right]. \tag{2.26}$$

Summing (2.26) for $j = 0, 1, \ldots, M-1$ and noticing (1.3), we get

$$\begin{aligned} \|\Phi^{n+1}\|_{l^2}^2 &= \|\Phi^n\|_{l^2}^2 - \frac{\tau h}{2\varepsilon}\sum_{j=0}^{M-1}\left[(\Phi_j^{n+1/2})^*\sigma_1\delta_x\Phi_j^{n+1/2} + (\Phi_j^{n+1/2})^T\sigma_1\delta_x\overline{\Phi}_j^{n+1/2}\right] \\ &= \|\Phi^n\|_{l^2}^2 - \frac{\tau}{2\varepsilon}\sum_{j=0}^{M-1}\Big[(\Phi_j^{n+1/2})^*\sigma_1\Phi_{j+1}^{n+1/2} + (\Phi_j^{n+1/2})^T\sigma_1\overline{\Phi}_{j+1}^{n+1/2} \\ &\qquad -(\Phi_{j+1}^{n+1/2})^*\sigma_1\Phi_j^{n+1/2} - (\Phi_{j+1}^{n+1/2})^T\sigma_1\overline{\Phi}_j^{n+1/2}\Big] \\ &= \|\Phi^n\|_{l^2}^2, \quad n \geq 0, \end{aligned} \tag{2.27}$$

which immediately implies (2.24) by induction.

(ii) Secondly, we prove the energy conservation (2.25). Multiplying both sides of (2.9) from left by $2h\,(\Phi_j^{n+1}-\Phi_j^n)^*$ and taking the real part, we have

$$-h\,\mathrm{Re}\left[\frac{i}{\varepsilon}(\Phi_j^{n+1}-\Phi_j^n)^*\sigma_1\delta_x(\Phi_j^{n+1}+\Phi_j^n)\right]+\frac{h}{\varepsilon^2}\left[(\Phi_j^{n+1})^*\sigma_3\Phi_j^{n+1}-(\Phi_j^n)^*\sigma_3\Phi_j^n\right]$$
$$+hV_j(|\Phi_j^{n+1}|^2-|\Phi_j^n|^2)-hA_{1,j}\left[(\Phi_j^{n+1})^*\sigma_1\Phi_j^{n+1}-(\Phi_j^n)^*\sigma_1\Phi_j^n\right]=0. \tag{2.28}$$

Summing (2.28) for $j=0,1,\ldots,M-1$ and noticing the summation by parts formula, we have

$$h\sum_{j=0}^{M-1}\mathrm{Re}\left(\frac{i}{\varepsilon}(\Phi_j^{n+1}-\Phi_j^n)^*\sigma_1\delta_x(\Phi_j^{n+1}+\Phi_j^n)\right)$$
$$=\frac{ih}{\varepsilon}\sum_{j=0}^{M-1}(\Phi_j^{n+1})^*\sigma_1\delta_x\Phi_j^{n+1}-\frac{ih}{\varepsilon}\sum_{j=0}^{M-1}(\Phi_j^n)^*\sigma_1\delta_x\Phi_j^n,$$

and

$$-\frac{ih}{\varepsilon}\sum_{j=0}^{M-1}(\Phi_j^{n+1})^*\sigma_1\delta_x\Phi_j^{n+1}+\frac{ih}{\varepsilon}\sum_{j=0}^{M-1}(\Phi_j^n)^*\sigma_1\delta_x\Phi_j^n$$
$$+\frac{h}{\varepsilon^2}\sum_{j=0}^{M-1}\left((\Phi_j^{n+1})^*\sigma_3\Phi_j^{n+1}-(\Phi_j^n)^*\sigma_3\Phi_j^n\right)+h\sum_{j=0}^{M-1}V_j(|\Phi_j^{n+1}|^2-|\Phi_j^n|^2)$$
$$-h\sum_{j=0}^{M-1}A_{1,j}\left((\Phi_j^{n+1})^*\sigma_1\Phi_j^{n+1}-(\Phi_j^n)^*\sigma_1\Phi_j^n\right)=0, \tag{2.29}$$

which immediately implies (2.25). □

2.4 Error Estimates

Let $0<T<T^*$ with T^* being the maximal existence time of the solution, and denote $\Omega_T=[0,T]\times\Omega$. Motivated by the nonrelativistic limit of the Dirac equation [18] and the dispersion relation (1.26), we assume that the exact solution of (2.1) satisfies $\Phi\in C^3([0,T];(L^\infty(\Omega))^2)\cap C^2([0,T];(W_p^{1,\infty}(\Omega))^2)\cap C^1([0,T];(W_p^{2,\infty}(\Omega))^2)\cap C([0,T];(W_p^{3,\infty}(\Omega))^2)$ and

$$(A)\quad \left\|\frac{\partial^{r+s}}{\partial t^r\partial x^s}\Phi\right\|_{L^\infty([0,T];(L^\infty(\Omega))^2)}\lesssim\frac{1}{\varepsilon^{2r}},\ 0\le r\le 3,\ 0\le r+s\le 3,\ 0<\varepsilon\le 1, \tag{2.30}$$

where $W_p^{m,\infty}(\Omega)=\{u\mid u\in W^{m,\infty}(\Omega),\ \partial_x^l u(a)=\partial_x^l u(b),\ l=0,\ldots,m-1\}$ for $m\ge 1$ and here the boundary values are understood in the trace sense. In the subsequent discussion, we will omit Ω when referring to the space norm taken on Ω. In addition, we assume the electromagnetic potentials $V\in C(\overline{\Omega}_T)$ and $A_1\in C(\overline{\Omega}_T)$ and denote

$$(B)\qquad V_{\max}:=\max_{(t,x)\in\overline{\Omega}_T}|V(t,x)|,\quad A_{1,\max}:=\max_{(t,x)\in\overline{\Omega}_T}|A_1(t,x)|. \tag{2.31}$$

Remark 2.1 From the analysis point of view, if $V(t,x)$, $A_1(t,x)$ and initial data Φ_0 are sufficiently smooth, e.g. $V(t,x),A(t,x)\in C([0,T];W_p^{4,2})\cap C^1([0,T];W_p^{2,2})\cap$

$C^2([0,T];W_p^{1,2})$ and $\Phi_0 \in (W_p^{4,2})^2$, the assumption (A) would hold [18]. In practice, if the exact solution $\Phi(t,x)$ remains well localized for $t < T$ and the errors due to the periodic truncation of $V(t,x)\Phi(t,x)$ and $A_1(t,x)\Phi(t,x)$ onto the bounded domain Ω are negligible, the error estimates presented below would still hold without the periodicity assumptions on $V(t,x)$, $A_1(t,x)$ and Φ_0. It is worth noticing that the honeycomb lattice potential [3] and many other external electromagnetic potentials have the desired smoothness.

Define the grid error function $\mathbf{e}^n = (\mathbf{e}_0^n, \mathbf{e}_1^n, \ldots, \mathbf{e}_M^n)^T \in X_M$ as:

$$\mathbf{e}_j^n = \Phi(t_n, x_j) - \Phi_j^n, \quad j = 0, 1, \ldots, M, \quad n \geq 0, \tag{2.32}$$

with Φ_j^n being the approximations obtained from the FDTD methods.

For the LFFD (2.6), we assume the stability condition

$$0 < \tau \leq \frac{\varepsilon^2 h}{\varepsilon^2 h V_{\max} + \sqrt{h^2 + \varepsilon^2 (1 + \varepsilon h A_{1,\max})^2}}, \quad h > 0, \quad 0 < \varepsilon \leq 1, \tag{2.33}$$

and establish the following error estimate (see its proof in "Appendix 1").

Theorem 2.1 *Under the assumptions (A) and (B), there exist constants $h_0 > 0$ and $\tau_0 > 0$ sufficiently small and independent of ε, such that for any $0 < \varepsilon \leq 1$, when $0 < h \leq h_0$ and $0 < \tau \leq \tau_0$ and under the stability condition (2.33), we have the following error estimate for the LFFD (2.6) with (2.10) and (2.11)*

$$\|\mathbf{e}^n\|_{l^2} \lesssim \frac{h^2}{\varepsilon} + \frac{\tau^2}{\varepsilon^6}, \quad 0 \leq n \leq \frac{T}{\tau}. \tag{2.34}$$

Similar to the proof of the LFFD method, error estimates for the CNFD (2.9), SIFD1 (2.7) and SIFD2 (2.8) under the stability condition

$$0 < \tau \leq \frac{1}{V_{\max} + A_{1,\max}}, \quad h > 0, \quad 0 < \varepsilon \leq 1, \tag{2.35}$$

can be derived and the details are omitted here for brevity.

Theorem 2.2 *Under the assumptions (A) and (B), there exist constants $h_0 > 0$ and $\tau_0 > 0$ sufficiently small and independent of ε, such that for any $0 < \varepsilon \leq 1$, $0 < h \leq h_0$ and $0 < \tau \leq \tau_0$, we have the following error estimate for the CNFD (2.9) with (2.10)*

$$\|\mathbf{e}^n\|_{l^2} \lesssim \frac{h^2}{\varepsilon} + \frac{\tau^2}{\varepsilon^6}, \quad 0 \leq n \leq \frac{T}{\tau}. \tag{2.36}$$

Theorem 2.3 *Under the assumptions (A) and (B), there exist constants $h_0 > 0$ and $\tau_0 > 0$ sufficiently small and independent of ε, such that for any $0 < \varepsilon \leq 1$, when $0 < h \leq h_0$ and $0 < \tau \leq \tau_0$ and under the stability condition (2.14), we have the following error estimate for the SIFD1 (2.7) with (2.10) and (2.11)*

$$\|\mathbf{e}^n\|_{l^2} \lesssim \frac{h^2}{\varepsilon} + \frac{\tau^2}{\varepsilon^6}, \quad 0 \leq n \leq \frac{T}{\tau}. \tag{2.37}$$

Theorem 2.4 *Under the assumptions (A) and (B), there exist constants $h_0 > 0$ and $\tau_0 > 0$ sufficiently small and independent of ε, such that for any $0 < \varepsilon \leq 1$, when $0 < h \leq h_0$ and $0 < \tau \leq \tau_0$ and under the stability condition (2.35), we have the following error estimate for the SIFD2 (2.8) with (2.10) and (2.11)*

$$\|\mathbf{e}^n\|_{l^2} \lesssim \frac{h^2}{\varepsilon} + \frac{\tau^2}{\varepsilon^6}, \quad 0 \leq n \leq \frac{T}{\tau}. \tag{2.38}$$

Based on Theorems 2.2–2.4, the four FDTD methods studied here share the same temporal/spatial resolution capacity in the nonrelativistic limit regime. In fact, given an accuracy bound $\delta > 0$, the ε-scalability of the four FDTD methods is:

$$\tau = O\left(\varepsilon^3\sqrt{\delta}\right) = O(\varepsilon^3), \quad h = O\left(\sqrt{\delta\varepsilon}\right) = O\left(\sqrt{\varepsilon}\right), \quad 0 < \varepsilon \ll 1. \tag{2.39}$$

3 A sEWI-FP Method and Its Analysis

In this section, we propose a symmetric exponential wave integrator Fourier pseudospectral (sEWI-FP) method to solve the Dirac equation (1.9) (or 1.21) and establish its stability and convergence in the nonrelativistic limit regime. Again, for simplicity of notations, we shall only present the numerical method and its analysis for (2.1) in 1D. Generalization to (1.9) and/or higher dimensions is straightforward and the results remain valid without modifications (see generalizations in "Appendix 3").

3.1 The sEWI-FP Method

Denote

$$Y_M = Z_M \times Z_M, \ Z_M = \text{span}\left\{\phi_l(x) = e^{i\mu_l(x-a)}, \ l = -\frac{M}{2}, \ldots, \frac{M}{2}-1\right\}.$$

Let $[C_p(\overline{\Omega})]^2$ be the function space consisting of all periodic vector function $U(x) : \overline{\Omega} = [a, b] \to \mathbb{C}^2$. For any $U(x) \in [C_p(\overline{\Omega})]^2$ and $U \in X_M$, define $P_M : [L^2(\Omega)]^2 \to Y_M$ as the standard projection operator [70], $I_M : [C_p(\overline{\Omega})]^2 \to Y_M$ and $I_M : X_M \to Y_M$ as the standard interpolation operator [70], i.e. for $a \le x \le b$

$$(P_M U)(x) = \sum_{l=-M/2}^{M/2-1} \widehat{U}_l \, e^{i\mu_l(x-a)}, \quad (I_M U)(x) = \sum_{l=-M/2}^{M/2-1} \widetilde{U}_l \, e^{i\mu_l(x-a)}, \tag{3.1}$$

with

$$\widehat{U}_l = \frac{1}{b-a}\int_a^b U(x)\, e^{-i\mu_l(x-a)}\, dx, \quad \widetilde{U}_l = \frac{1}{M}\sum_{j=0}^{M-1} U_j \, e^{-2ijl\pi/M}, \tag{3.2}$$

where $l = -\frac{M}{2}, -\frac{M}{2}+1, \ldots, \frac{M}{2}-1$ and $U_j = U(x_j)$ when U is a function.

The Fourier spectral discretization for the Dirac equation (2.1) is as follows: Find $\Phi_M(t, x) \in Y_M$, i.e.

$$\Phi_M(t, x) = \sum_{l=-M/2}^{M/2-1} \widehat{(\Phi_M)}_l(t)\, e^{i\mu_l(x-a)}, \quad a \le x \le b, \quad t \ge 0, \tag{3.3}$$

such that, for $a < x < b$ and $t > 0$, $\Phi_M := \Phi_M(t, x)$ satisfies

$$i\,\partial_t \Phi_M = \left[-\frac{i}{\varepsilon}\sigma_1\partial_x + \frac{1}{\varepsilon^2}\sigma_3\right]\Phi_M + P_M(V\Phi_M)(t, x) - \sigma_1 P_M(A_1\Phi_M). \tag{3.4}$$

Substituting (3.3) into (3.4), noticing the orthogonality of $\phi_l(x)$, we get for $l = -\frac{M}{2}, \ldots, \frac{M}{2}-1$ and $t \ge 0$

$$i\,\frac{d}{dt}\widehat{(\Phi_M)}_l(t) = \left[\frac{\mu_l}{\varepsilon}\sigma_1 + \frac{1}{\varepsilon^2}\sigma_3\right]\widehat{(\Phi_M)}_l(t) + \widehat{(V\Phi_M)}_l(t) - \sigma_1\widehat{(A_1\Phi_M)}_l(t) = 0. \tag{3.5}$$

For each l ($l = -\frac{M}{2}, -\frac{M}{2}+1, \ldots, \frac{M}{2}-1$), when t is near $t = t_n$ ($n \geq 0$), we rewrite the above ODEs as

$$i\,\frac{d}{ds}\widehat{(\Phi_M)}_l(t_n+s) = \frac{1}{\varepsilon^2}\Gamma_l\,\widehat{(\Phi_M)}_l(t_n+s) + \widehat{F}_l^n(s), \quad s \in \mathbb{R}, \tag{3.6}$$

where

$$\widehat{F}_l^n(s) = \widehat{(G\Phi_M)}_l(t_n+s), \quad G(t,x) = V(t,x)I_2 - \sigma_1 A_1(t,x), \quad s,t \in \mathbb{R}, \tag{3.7}$$

and $\Gamma_l = \mu_l\varepsilon\sigma_1 + \sigma_3 = Q_l\,D_l\,(Q_l)^*$ with $\delta_l = \sqrt{1+\varepsilon^2\mu_l^2}$ and

$$\Gamma_l = \begin{pmatrix} 1 & \mu_l\varepsilon \\ \mu_l\varepsilon & -1 \end{pmatrix}, \quad Q_l = \begin{pmatrix} \frac{1+\delta_l}{\sqrt{2\delta_l(1+\delta_l)}} & -\frac{\varepsilon\mu_l}{\sqrt{2\delta_l(1+\delta_l)}} \\ \frac{\varepsilon\mu_l}{\sqrt{2\delta_l(1+\delta_l)}} & \frac{1+\delta_l}{\sqrt{2\delta_l(1+\delta_l)}} \end{pmatrix}, \quad D_l = \begin{pmatrix} \delta_l & 0 \\ 0 & -\delta_l \end{pmatrix}. \tag{3.8}$$

Solving the above ODE (3.6) via the integrating factor method, we obtain

$$\widehat{(\Phi_M)}_l(t_n+s) = e^{-is\Gamma_l/\varepsilon^2}\,\widehat{(\Phi_M)}_l(t_n) - i\int_0^s e^{i(w-s)\Gamma_l/\varepsilon^2}\,\widehat{F}_l^n(w)\,dw, \ s \in \mathbb{R}. \tag{3.9}$$

We note here that $e^{is\Gamma_l} = \cos(s\Gamma_l) + i\sin(s\Gamma_l)$ ($s \in \mathbb{R}, l = -\frac{M}{2}, \ldots, M-1$) and

$$\sin(s\Gamma_l) = Q_l \begin{pmatrix} \sin(s\delta_l) & 0 \\ 0 & -\sin(s\delta_l) \end{pmatrix} Q_l^*, \quad \cos(s\Gamma_l) = \cos(s\delta_l)I_2. \tag{3.10}$$

Setting $n = 0$ and $s = \tau$, we get

$$\widehat{(\Phi_M)}_l(\tau) = e^{-is\Gamma_l/\varepsilon^2}\,\widehat{(\Phi_M)}_l(0) - i\int_0^\tau e^{i(w-\tau)\Gamma_l/\varepsilon^2}\,\widehat{F}_l^0(w)\,dw. \tag{3.11}$$

For $n \geq 1$, taking $s = \tau$ and $s = -\tau$ in (3.9), respectively, and subtracting one from the other, we have

$$\begin{aligned} \widehat{(\Phi_M)}_l(t_{n+1}) =& \widehat{(\Phi_M)}_l(t_{n-1}) - 2i\sin(\tau\Gamma_l/\varepsilon^2)\widehat{(\Phi_M)}_l(t_n) \\ & - i\int_0^\tau \cos\left(\frac{(w-\tau)\delta_l}{\varepsilon^2}\right)\left(\widehat{F}_l^n(w) + \widehat{F}_l^n(-w)\right)dw \\ & + \int_0^\tau \sin\left(\frac{(w-\tau)\Gamma_l}{\varepsilon^2}\right)\left(\widehat{F}_l^n(w) - \widehat{F}_l^n(-w)\right)dw, \end{aligned} \tag{3.12}$$

To obtain an explicit numerical method with second order accuracy in time, we approximate the integrals in (3.11) and (3.12) via the Gautschi-type/trapezoidal rules [42,50,51], which have been widely used for integrating highly oscillatory ODEs [6,12,42,50,51,55,56], as

$$\begin{aligned} \int_0^\tau e^{\frac{i(w-\tau)}{\varepsilon^2}\Gamma_l}\,\widehat{F}_l^0(w)\,dw &\approx \int_0^\tau e^{\frac{i(w-\tau)}{\varepsilon^2}\Gamma_l}\,dw\,\widehat{F}_l^0(0) \\ &= -i\varepsilon^2\Gamma_l^{-1}\left[I_2 - e^{-\frac{i\tau}{\varepsilon^2}\Gamma_l}\right]\widehat{F}_l^0(0), \end{aligned} \tag{3.13}$$

and for $n \geq 1$

$$\int_0^\tau \cos\left(\frac{(w-\tau)}{\varepsilon^2}\delta_l\right)\left(\widehat{F}_l^n(w)+\widehat{F}_l^n(-w)\right)dw$$
$$\approx \int_0^\tau \cos\left(\frac{(w-\tau)}{\varepsilon^2}\delta_l\right)\left(2\widehat{F}_l^n(0)+\partial_t\widehat{F}_l^n(0)(w-w)\right)dw = \frac{2\varepsilon^2}{\delta_l}\sin(\tau\delta_l/\varepsilon^2)\widehat{F}_l^n(0), \tag{3.14}$$

$$\int_0^\tau \sin((w-\tau)\Gamma_l/\varepsilon^2)\left(\widehat{F}_l^n(w)-\widehat{F}_l^n(-w)\right)dw$$
$$\approx \frac{\tau}{2}\left[\sin\left(\frac{-\tau\Gamma_l}{\varepsilon^2}\right)\mathbf{0}+\sin\left(\frac{0\Gamma_l}{\varepsilon^2}\right)\left(\widehat{F}_l^n(\tau)-\widehat{F}_l^n(-\tau)\right)\right]=\mathbf{0}. \tag{3.15}$$

Now, we are ready to describe our scheme. Let $\Phi_M^n(x)$ be the approximation of $\Phi_M(t_n,x)$ $(n\geq 0)$. Choosing $\Phi_M^0(x)=(P_M\Phi_0)(x)$, a *symmetric exponential wave integrator Fourier spectral* (sEWI-FS) discretization for the Dirac equation (2.1) is to update the numerical approximation $\Phi_M^{n+1}(x)\in Y_M$ $(n=0,1,\ldots)$ as

$$\Phi_M^{n+1}(x)=\sum_{l=-M/2}^{M/2-1}\widehat{(\Phi_M^{n+1})}_l\, e^{i\mu_l(x-a)},\quad a\leq x\leq b,\quad n\geq 0, \tag{3.16}$$

where for $l=-\frac{M}{2},\ldots,\frac{M}{2}-1$,

$$\widehat{(\Phi_M^{n+1})}_l=\begin{cases} e^{-i\tau\Gamma_l/\varepsilon^2}\widehat{(\Phi_M^0)}_l-\varepsilon^2\Gamma_l^{-1}\left[I_2-e^{-\frac{i\tau}{\varepsilon^2}\Gamma_l}\right]\widehat{(G(t_0)\Phi_M^0)}_l, & n=0,\\ -2i\sin(\tau\Gamma_l/\varepsilon^2)\,\widehat{(\Phi_M^n)}_l+\widehat{(\Phi_M^{n-1})}_l-i\frac{2\varepsilon^2}{\delta_l}\sin(\frac{\tau\delta_l}{\varepsilon^2})\widehat{(G(t_n)\Phi_M^n)}_l, & n\geq 1,\end{cases} \tag{3.17}$$

with $G(t):=G(t,x)$. Notice that the above scheme for $n\geq 1$ is unchanged if we interchange $n+1\leftrightarrow n-1$ and $\tau\leftrightarrow-\tau$.

The above procedure is not suitable in practice due to the difficulty in computing the Fourier coefficients through integrals in (3.2). Here we present an efficient implementation by choosing $\Phi_M^0(x)$ as the interpolant of $\Phi_0(x)$ on the grids $\{x_j, j=0,1,\ldots,M\}$ and approximate the integrals in (3.2) by a quadrature rule.

Let Φ_j^n be the numerical approximation of $\Phi(t_n,x_j)$ for $j=0,1,2,\ldots,M$ and $n\geq 0$, and denote $\Phi^n\in X_M$ as the vector with components Φ_j^n. Choosing $\Phi_j^0=\Phi_0(x_j)$ $(j=0,1,\ldots,M)$, the *sEWI Fourier pseudospectral* (sEWI-FP) method for computing Φ^{n+1} for $n\geq 0$ reads

$$\Phi_j^{n+1}=\sum_{l=-M/2}^{M/2-1}\widetilde{(\Phi^{n+1})}_l e^{2ijl\pi/M},\quad j=0,1,\ldots,M, \tag{3.18}$$

where

$$\widetilde{(\Phi^{n+1})}_l=\begin{cases} e^{-i\tau\Gamma_l/\varepsilon^2}\widetilde{(\Phi_0)}_l-\varepsilon^2\Gamma_l^{-1}\left[I_2-e^{-\frac{i\tau}{\varepsilon^2}\Gamma_l}\right]\widetilde{(G(t_0)\Phi_0)}_l, & n=0,\\ -2i\sin(\tau\Gamma_l/\varepsilon^2)\,\widetilde{(\Phi^n)}_l+\widetilde{(\Phi^{n-1})}_l-i\frac{2\varepsilon^2}{\delta_l}\sin(\frac{\tau\delta_l}{\varepsilon^2})\widetilde{(G(t_n)\Phi^n)}_l, & n\geq 1.\end{cases} \tag{3.19}$$

The sEWI-FP (3.18–3.19) is explicit, and can be computed efficiently by the fast Fourier transform (FFT). The memory cost is $O(M)$ and the computational cost per time step is $O(M\log M)$.

3.2 Linear Stability Analysis

To consider the linear stability, we assume that in the Dirac equation (2.1), the external potential fields are constants, i.e. $A_1(t,x) \equiv A_1^0$ and $V(t,x) \equiv V^0$ with A_1^0 and V^0 being two real constants. Then we have

Lemma 3.1 *The sEWI-FP method* (3.18)–(3.19) *and sEWI-FS method* (3.16)–(3.17) *are stable under the condition*

$$0 < \tau \le \min\left\{ \frac{h\varepsilon^2\pi}{3\sqrt{h^2+\varepsilon^2\pi^2}}, \frac{2-\sqrt{3}}{2(|V^0|+|A_1^0|)} \right\}, \quad 0 < \varepsilon \le 1. \tag{3.20}$$

Proof We shall only prove the sEWI-FP case (3.19), as the sEWI-FP method case (3.16–3.17) is quite the same.

Similarly to the proof of Lemma 2.1, noticing (3.17), (3.7), (3.12) and (3.14), we find that

$$\xi_l^2(\widetilde{\Phi^0})_l = -2i\xi_l \sin(\tau\Gamma_l/\varepsilon^2)(\widetilde{\Phi^0})_l + (\widetilde{\Phi^0})_l - 2i\xi_l\varepsilon^2\delta_l^{-1}\sin(\tau\delta_l/\varepsilon^2)(V^0 I_2 - A_1^0\sigma_1)(\widetilde{\Phi^0})_l. \tag{3.21}$$

Multiplying both sides of (3.21) by $\overline{\xi_l}(\widetilde{\Phi^0})_l^*$ and then taking the real part and dividing both sides by $(\widetilde{\Phi^0})_l^*(\widetilde{\Phi^0})_l$, in view of Hermitian matrices Γ_l, σ_1, we get

$$|\xi_l|^2 \mathrm{Re}(\xi_l) = \mathrm{Re}(\overline{\xi_l}), \tag{3.22}$$

which implies $|\xi_l| = 1$ if $\mathrm{Re}(\xi_l) \neq 0$. On the other hand, if $\mathrm{Re}(\xi_l) = 0$, we can take $\xi_l = ic_l$ with $c_l \in \mathbb{R}$, and (3.21) leads to

$$-c_l^2(\widetilde{\Phi^0})_l = 2c_l \sin(\tau\Gamma_l/\varepsilon^2)(\widetilde{\Phi^0})_l + (\widetilde{\Phi^0})_l + 2c_l\varepsilon^2\delta_l^{-1}\sin(\tau\delta_l/\varepsilon^2)(V^0 I_2 - A_1^0\sigma_1)(\widetilde{\Phi^0})_l. \tag{3.23}$$

Denoting $C = |V^0| + |A_1^0|$, multiplying both sides of (3.23) by $(\widetilde{\Phi^0})_l^*$ and then dividing both sides by $(\widetilde{\Phi^0})_l^*(\widetilde{\Phi^0})_l$, noticing $\sin(\tau\delta_l/\varepsilon^2) \le \frac{\sqrt{3}}{2}$ under the stability constraint and $|\varepsilon^2\delta_l^{-1}\sin(\tau\delta_l/\varepsilon^2)| \le \tau$, we obtain

$$c_l^2 + 1 \le \sqrt{3}|c_l| + 2\tau C|c_l|, \tag{3.24}$$

where no real number c_l can satisfy the above inequality if $\tau < \frac{2-\sqrt{3}}{2C}$. It follows that the sEWI-FS (3.16–3.17) is stable under the constraint (3.20). □

3.3 Error Estimates

In order to obtain an error estimate for the sEWI methods (3.16–3.17) and (3.18–3.19), motivated by the results in [19,24], we assume that there exists an integer $m_0 \ge 2$ such that the exact solution $\Phi(t,x)$ of the Dirac equation (2.1) satisfies

$$(C) \qquad \|\Phi\|_{L^\infty([0,T];(H_p^{m_0})^2)} \lesssim 1, \ \|\partial_t^s \Phi\|_{L^\infty([0,T];(L^2)^2)} \lesssim \frac{1}{\varepsilon^{2s}}, \quad s = 1, 2,$$

where $H_p^k(\Omega) = \{u \mid u \in H^k(\Omega),\ \partial_x^l u(a) = \partial_x^l u(b),\ l = 0, \ldots, k-1\}$. In addition, we assume the electromagnetic potentials satisfy

$$(D) \qquad \|V\|_{W^{2,\infty}([0,T];L^\infty)} + \|A_1\|_{W^{2,\infty}([0,T];L^\infty)} \lesssim 1.$$

The following estimate can be established (see its proof in "Appendix 2").

Theorem 3.1 *Let $\Phi_M^n(x)$ be the approximation obtained from the sEWI-FS (3.16)–(3.17). Under the assumptions (C) and (D), there exists $h_0 > 0$ and $\tau_0 > 0$ sufficiently small and independent of ε such that, for any $0 < \varepsilon \leq 1$ under the stability constraint*

$$0 < \tau \leq \frac{h\varepsilon^2\pi}{3\sqrt{h^2+\varepsilon^2\pi^2}}, \tag{3.25}$$

when $0 < h \leq h_0$ and $0 < \tau \leq \tau_0$ satisfying the stability condition (3.25), we have the following error estimate

$$\|\Phi(t_n,x) - \Phi_M^n(x)\|_{L^2} \lesssim \frac{\tau^2}{\varepsilon^4} + h^{m_0}, \quad 0 \leq n \leq \frac{T}{\tau}. \tag{3.26}$$

Remark 3.1 If we apply a filter in sEWI-FS (3.16–3.17), where we modify the coefficients in front of $(\widehat{\Phi_M^n})_l$ as $-2i\sin(\tau\Gamma_l/\varepsilon^2) \to -2i\cos(\tau\delta_l/\varepsilon^2)\sin(\tau\Gamma_l/\varepsilon^2)$, the resulting scheme will be stable for $\tau \lesssim 1$, i.e. the stability will be independent of ε and h. Accordingly, the error estimates will become $\tau^2/\varepsilon^6 + h^{m_0}$ under proper regularity assumptions on the exact solution.

Remark 3.2 The same error estimate in Theorem 3.1 holds for the sEWI-FP (3.18–3.19) and the proof is quite similar to that of Theorem 3.1.

4 A TSFP Method and Its Analysis

In this section, we present a time-splitting Fourier pseudospectral (TSFP) method to solve the Dirac equation(1.9) (or 1.21) which has been proposed and studied for the Maxwell–Dirac equation [17,53]. Again, for simplicity of notations, we shall only present the numerical method and its analysis for (2.1) in 1D. Generalization to (1.9) and/or higher dimensions is straightforward and results remain valid without modifications (see generalizations in "Appendix 3").

From time $t = t_n$ to time $t = t_{n+1}$, the Dirac equation (2.1) is split into two steps. One solves first

$$i\partial_t\Phi(t,x) = \left[-\frac{i}{\varepsilon}\sigma_1\partial_x + \frac{1}{\varepsilon^2}\sigma_3\right]\Phi(t,x), \quad x \in \Omega, \tag{4.1}$$

with the periodic boundary condition (2.2) for the time step of length τ, followed by solving

$$i\partial_t\Phi(t,x) = [-A_1(t,x)\sigma_1 + V(t,x)I_2]\,\Phi(t,x), \quad x \in \Omega, \tag{4.2}$$

for the same time step. Equation (4.1) will be first discretized in space by the Fourier spectral method and then integrated (in phase or Fourier space) in time *exactly* [17]. For the ODEs (4.2), we can integrate *analytically* in time as

$$\Phi(t,x) = e^{-i\int_{t_n}^{t}[V(s,x)\,I_2 - A_1(s,x)\,\sigma_1]ds}\,\Phi(t_n,x), \ a \leq x \leq b, \ t_n \leq t \leq t_{n+1}. \tag{4.3}$$

In practical computation, from time $t = t_n$ to $t = t_{n+1}$, one often combines the splitting steps via the standard Strang splitting [73]—which results in a second order time-splitting Fourier

pseudospectral (TSFP) method—as

$$\Phi_j^{(1)} = \sum_{l=-\frac{M}{2}}^{M/2-1} e^{-i\frac{\tau\Gamma_l}{2\varepsilon^2}}\,\widetilde{(\Phi^n)}_l\, e^{i\mu_l(x_j-a)} = \sum_{l=-\frac{M}{2}}^{\frac{M}{2}-1} Q_l\, e^{-i\frac{\tau D_l}{2\varepsilon^2}}\,(Q_l)^*\,\widetilde{(\Phi^n)}_l\, e^{\frac{2ijl\pi}{M}},$$

$$\Phi_j^{(2)} = e^{-i\int_{t_n}^{t_{n+1}} G(t,x_j)\,dt}\,\Phi_j^{(1)} = P_j\, e^{-i\Lambda_j}\, P_j^*\,\Phi_j^{(1)}, \quad 0\le j\le M,\ n\ge 0, \tag{4.4}$$

$$\Phi_j^{n+1} = \sum_{l=-\frac{M}{2}}^{\frac{M}{2}-1} e^{-i\frac{\tau\Gamma_l}{2\varepsilon^2}}\,\widetilde{(\Phi^{(2)})}_l\, e^{i\mu_l(x_j-a)} = \sum_{l=-\frac{M}{2}}^{\frac{M}{2}-1} Q_l\, e^{-i\frac{\tau D_l}{2\varepsilon^2}}\,(Q_l)^*\,\widetilde{(\Phi^{(2)})}_l\, e^{\frac{2ijl\pi}{M}},$$

where $\int_{t_n}^{t_{n+1}} G(t,x_j)dt = V_j^{(1)} I_2 - A_{1,j}^{(1)}\sigma_1 = P_j\,\Lambda_j\,P_j^*$ with $V_j^{(1)} = \int_{t_n}^{t_{n+1}} V(t,x_j)dt$, $A_{1,j}^{(1)} = \int_{t_n}^{t_{n+1}} A_1(t,x_j)dt$, $\Lambda_j = \mathrm{diag}(\Lambda_{j,+},\Lambda_{j,-})$ with $\Lambda_{j,\pm} = V_j^{(1)} \pm A_{1,j}^{(1)}$, and $P_j = I_2$ if $A_{1,j}^{(1)} = 0$ and otherwise

$$P_j = P^{(0)} := \begin{pmatrix} \frac{1}{\sqrt{2}} & -\frac{1}{\sqrt{2}} \\ \frac{1}{\sqrt{2}} & \frac{1}{\sqrt{2}} \end{pmatrix}. \tag{4.5}$$

Remark 4.1 Again, if the definite integrals in $\int_{t_n}^{t_{n+1}} \Lambda(t,x_j)\,dt$ cannot be evaluated analytically, we can evaluate them numerically via the Simpson's quadrature rule as

$$\int_{t_n}^{t_{n+1}} A_1(t,x_j)\,dt \approx \frac{\tau}{6}\left[A_1(t_n,x_j) + 4A_1\left(t_n+\frac{\tau}{2},x_j\right) + A_1(t_{n+1},x_j)\right],$$

$$\int_{t_n}^{t_{n+1}} V(t,x_j)\,dt \approx \frac{\tau}{6}\left[V(t_n,x_j) + 4V\left(t_n+\frac{\tau}{2},x_j\right) + V(t_{n+1},x_j)\right].$$

Lemma 4.1 *The TSFP* (4.4) *conserves the mass in the discretized level, i.e.*

$$\|\Phi^n\|_{l^2}^2 := h\sum_{j=0}^{M-1}|\Phi_j^n|^2 \equiv h\sum_{j=0}^{M-1}|\Phi_j^0|^2 = \|\Phi^0\|_{l^2}^2 = h\sum_{j=0}^{M-1}|\Phi_0(x_j)|^2, \quad n\ge 0. \tag{4.6}$$

Proof The proof is quite standard and similar to that of Lemma 2.2. We omit it here. □

From Lemma 4.1, we conclude that the TSFP (4.4) is unconditionally stable. In addition, under proper assumptions of the exact solution $\Phi(t,x)$ and electromagnetic potentials, it is easy to show the following error estimate via the formal Lie calculus introduced in [58],

$$\|\Phi(t_n,x) - I_M(\Phi^n)\|_{L^2} \lesssim h^{m_0} + \frac{\tau^2}{\varepsilon^4}, \quad 0\le n\le \frac{T}{\tau}, \tag{4.7}$$

where m_0 depends on the regularity of $\Phi(t,x)$. We omit the details here for brevity.

5 Numerical Comparison and Applications

In this section, we compare the accuracy of different numerical methods including the FDTD, sEWI-FP and TSFP methods for the Dirac equation (1.21) in 1D in terms of the mesh size h, time step τ and the parameter $0<\varepsilon\le 1$. We will pay particular attention to the ε-scalability of different methods in the nonrelativistic limit regime, i.e. $0<\varepsilon\ll 1$. Then we simulate the dynamics of the Dirac equation (1.21) in 2D with a honeycomb lattice potential by the TSFP method.

5.1 Comparison of Spatial/Temporal Resolution

To test the accuracy, we choose the electromagnetic potentials in the Dirac equation (1.21) with $d = 1$ as

$$A_1(t,x) = \frac{(x+1)^2}{1+x^2}, \quad V(t,x) = \frac{1-x}{1+x^2}, \quad x \in \mathbb{R}, \quad t \geq 0, \tag{5.1}$$

and the initial data as

$$\phi_1(0,x) = e^{-x^2/2}, \quad \phi_2(0,x) = e^{-(x-1)^2/2}, \quad x \in \mathbb{R}. \tag{5.2}$$

The problem is solved numerically on an interval $\Omega = (-16, 16)$ with periodic boundary conditions on $\partial\Omega$. The 'reference' solution $\Phi(t,x) = (\phi_1(t,x), \phi_2(t,x))^T$ is obtained numerically by using the TSFP method with a small time step and a very fine mesh size, e.g. $\tau_e = 10^{-7}$ and $h_e = 1/16$ or $h_e = 1/4096$ for the comparison of the sEWI-FP/TSFP methods or the FDTD methods, respectively. Denote $\Phi^n_{h,\tau}$ as the numerical solution obtained by a numerical method with mesh size h and time step τ. In order to quantify the convergence, we introduce

$$e_{h,\tau}(t_n) = \|\Phi^n - \Phi(t_n,\cdot)\|_{l^2} = \sqrt{h \sum_{j=0}^{M-1} |\Phi^n_j - \Phi(t_n, x_j)|^2}.$$

Table 1 lists spatial errors $e_{h,\tau_e}(t=2)$ with different h (upper part) and temporal errors $e_{h_e,\tau}(t=2)$ with different τ (lower part) for the LFFD method (2.6). Tables 2, 3, 4, 5 and 6 show similar results for the SIFD1 method (2.7), SIFD2 method (2.8), CNFD method (2.9), sEWI-FP method (3.18–3.19) and TSFP method (4.4), respectively. For the LFFD and SIFD1 methods, due to the stability condition and accuracy requirement, we take

$$\delta_j(\varepsilon) = \begin{cases} \varepsilon^2, & \varepsilon_0/2^j \leq \varepsilon \leq 1, \\ \varepsilon_0^2/4^j, & 0 < \varepsilon < \varepsilon_0/2^j, \end{cases} \quad j = 0, 1, \ldots$$

in Tables 1 and 2. For comparison, Table 7 depicts temporal errors of different numerical methods when $\varepsilon = 1$ for different τ, Table 8 depicts temporal errors of different numerical methods under different ε-scalability.

From Tables 1, 2, 3, 4, 5, 6, 7, and 8, and additional numerical results not shown here for brevity, we can draw the following conclusions for the Dirac equation by using different numerical methods:

(i). For the discretization error in space, for any fixed $\varepsilon = \varepsilon_0 > 0$, the FDTD methods are second-order accurate, and resp., the sEWI-FP and TSFP methods are spectrally accurate (cf. each row in the upper parts of Tables 1, 2, 3, 4, 5, 6 and 7). For $0 < \varepsilon \leq 1$, the errors are independent of ε for the sEWI-FP and TSFP methods (cf. each column in the upper parts of Tables 5, 6), and resp., are almost independent of ε for the FDTD methods (cf. each column in the upper parts of Tables 1, 2, 3, 4). In general, for any fixed $0 < \varepsilon \leq 1$ and $h > 0$, the sEWI-FP and TSFP methods perform much better than the FDTD methods in spatial discretization.

(ii). For the discretization error in time, in the $O(1)$ speed-of-light regime, i.e. $\varepsilon = O(1)$, all the numerical methods including FDTD, sEWI-FP and TSFP are second-order accurate (cf. the first row in the lower parts of Tables 1, 2, 3, 4, 5, 6). In general, the sEWI-FP and TSFP methods perform much better than the FDTD methods in temporal discretizations for a fixed time step. In the non-relativistic limit regime, i.e. $0 < \varepsilon \ll 1$, for the FDTD methods,

Table 1 Spatial and temporal error analysis of the LFFD method for the Dirac equation (1.21) in 1D

Spatial errors	$h_0 = 1/8$	$h_0/2$	$h_0/2^2$	$h_0/2^3$	$h_0/2^4$
$\varepsilon_0 = 1$	1.06E−1	2.65E−2	6.58E−3	1.64E−3	4.10E−4
Order	–	2.00	2.01	2.00	2.00
$\varepsilon_0/2$	9.06E−2	2.26E−2	5.64E−3	1.41E−3	3.51E−4
Order	–	2.00	2.00	2.00	2.01
$\varepsilon_0/2^2$	8.03E−2	2.02E−2	5.04E−3	1.25E−3	3.05E−4
Order	–	1.99	2.00	2.01	2.04
$\varepsilon_0/2^3$	9.89E−2	2.47E−2	6.17E−3	1.54E−3	3.85E−4
Order	–	2.00	2.00	2.00	2.00
$\varepsilon_0/2^4$	9.87E−2	2.48E−2	6.18E−3	1.54E−3	3.83E−4
Order	–	1.99	2.00	2.00	2.01
Temporal errors	$\tau_0 = 0.1$ $h_0 = 1/8$	$\tau_0/8$ $h_0/8\delta_1(\varepsilon)$	$\tau_0/8^2$ $h_0/8^2\delta_2(\varepsilon)$	$\tau_0/8^3$ $h_0/8^3\delta_3(\varepsilon)$	$\tau_0/8^4$ $h_0/8^4\delta_4(\varepsilon)$
$\varepsilon_0 = 1$	**1.38E−1**	1.99E−3	3.11E−5	4.86E−7	7.59E−9
Order	–	2.04	2.00	2.00	2.00
$\varepsilon_0/2$	Unstable	**1.14E−2**	1.77E−4	2.77E−6	4.32E−8
Order	–	–	2.00	2.00	2.00
$\varepsilon_0/2^2$	Unstable	4.59E−1	**7.01E−3**	1.05E−4	1.64E−6
Order	–	–	**2.01**	2.02	2.00
$\varepsilon_0/2^3$	Unstable	Unstable	4.14E−1	**6.42E−3**	1.00E−4
Order	–	–	–	**2.00**	2.00
$\varepsilon_0/2^4$	Unstable	Unstable	Unstable	4.04E−1	**6.00E−3**
Order	–	–	–	–	**2.02**

Table 2 Spatial and temporal error analysis of the SIFD1 method for the Dirac equation (1.21) in 1D

Spatial errors	$h_0 = 1/8$	$h_0/2$	$h_0/2^2$	$h_0/2^3$	$h_0/2^4$
$\varepsilon_0 = 1$	1.06E−1	2.65E−2	6.58E−3	1.64E−3	4.10E−4
Order	–	2.00	2.01	2.00	2.00
$\varepsilon_0/2$	9.06E−2	2.26E−2	5.64E−3	1.41E−3	3.51E−4
Order	–	2.00	2.00	2.00	2.01
$\varepsilon_0/2^2$	8.03E−2	2.02E−2	5.04E−3	1.25E−3	3.05E−4
Order	–	1.99	2.00	2.01	2.04
$\varepsilon_0/2^3$	9.89E−2	2.47E−2	6.17E−3	1.54E−3	3.85E−4
Order	–	2.00	2.00	2.00	2.00
$\varepsilon_0/2^4$	9.87E−2	2.48E−2	6.18E−3	1.54E−3	3.83E−4
Order	–	1.99	2.00	2.00	2.01

Table 2 continued

Temporal errors	$\tau_0 = 0.1$ $h_0 = 1/8$	$\tau_0/8$ $h_0/8\delta_1(\varepsilon)$	$\tau_0/8^2$ $h_0/8^2\delta_2(\varepsilon)$	$\tau_0/8^3$ $h_0/8^3\delta_3(\varepsilon)$	$\tau_0/8^4$ $h_0/8^4\delta_4(\varepsilon)$
$\varepsilon_0 = 1$	**1.44E−1**	2.09E−3	3.27E−5	5.11E−7	7.98E−9
Order	–	2.03	2.00	2.00	2.00
$\varepsilon_0/2$	Unstable	**2.99E−2**	4.67E−4	7.30E−6	1.14E−7
Order	–	–	2.00	2.00	2.00
$\varepsilon_0/2^2$	Unstable	8.18E−1	**1.54E−2**	2.41E−4	3.77E−6
Order	–	–	**1.91**	2.00	2.00
$\varepsilon_0/2^3$	Unstable	Unstable	7.99E−1	**1.31E−2**	2.05E−4
Order	–	–	–	**1.98**	2.00
$\varepsilon_0/2^4$	Unstable	Unstable	4.19E−1	7.97E−1	**1.26E−2**
Order	–	–	–	−0.31	**1.99**

Table 3 Spatial and temporal error analysis of the SIFD2 method for the Dirac equation (1.21) in 1D

Spatial errors	$h_0 = 1/8$	$h_0/2$	$h_0/2^2$	$h_0/2^3$	$h_0/2^4$
$\varepsilon_0 = 1$	1.06E−1	2.65E−2	6.58E−3	1.64E−3	4.10E−4
Order	–	2.00	2.01	2.00	2.00
$\varepsilon_0/2$	9.06E−2	2.26E−2	5.64E−3	1.41E−3	3.51E−4
Order	–	2.00	2.00	2.00	2.01
$\varepsilon_0/2^2$	8.03E−2	2.02E−2	5.04E−3	1.25E−3	3.05E−4
Order	–	1.99	2.00	2.01	2.04
$\varepsilon_0/2^3$	9.89E−2	2.47E−2	6.17E−3	1.54E−3	3.85E−4
Order	–	2.00	2.00	2.00	2.00
$\varepsilon_0/2^4$	9.87E−2	2.48E−2	6.18E−3	1.54E−3	3.83E−4
Order	–	1.99	2.00	2.00	2.01
Temporal errors	τ_0=0.1	$\tau_0/8$	$\tau_0/8^2$	$\tau_0/8^3$	$\tau_0/8^4$
$\varepsilon_0 = 1$	**1.72E−1**	2.59E−3	4.05E−5	6.33E−7	9.89E−9
Order	–	2.01	2.00	2.00	2.00
$\varepsilon_0/2$	1.69	**3.57E−2**	5.58E−4	8.72E−6	1.36E−7
Order	–	**1.86**	2.00	2.00	2.00
$\varepsilon_0/2^2$	2.59	8.66E−1	**1.63E−2**	2.55E−4	3.98E−6
Order	–	0.52	**1.91**	2.00	2.00
$\varepsilon_0/2^3$	2.67	2.89	8.43E−1	**1.37E−2**	2.14E−4
Order	–	−0.04	0.59	**1.98**	2.00
$\varepsilon_0/2^4$	3.07	3.56	5.19E−1	8.37E−1	**1.28E−2**
Order	–	−0.07	0.93	−0.23	**2.01**

Table 4 Spatial and temporal error analysis of the CNFD method for the Dirac equation (1.21) in 1D

Spatial errors	h_0=1/8	$h_0/2$	$h_0/2^2$	$h_0/2^3$	$h_0/2^3$
$\varepsilon_0 = 1$	1.06E−1	2.65E−2	6.58E−3	1.64E−3	4.10E−4
Order	–	2.00	2.01	2.00	2.00
$\varepsilon_0/2$	9.06E−2	2.26E−2	5.64E−3	1.41E−3	3.51E−4
Order	–	2.00	2.00	2.00	2.01
$\varepsilon_0/2^2$	8.03E−2	2.02E−2	5.04E−3	1.25E−3	3.05E−4
Order	–	1.99	2.00	2.01	2.04
$\varepsilon_0/2^3$	9.89E−2	2.47E−2	6.17E−3	1.54E−3	3.85E−4
Order	–	2.00	2.00	2.00	2.00
$\varepsilon_0/2^4$	9.87E−2	2.48E−2	6.18E−3	1.54E−3	3.83E−4
Order	–	1.99	2.00	2.00	2.01
Temporal errors	τ_0=0.1	$\tau_0/8$	$\tau_0/8^2$	$\tau_0/8^3$	$\tau_0/8^4$
$\varepsilon_0 = 1$	**5.48E−2**	8.56E−4	1.34E−5	2.09E−7	3.27E−9
Order	–	2.00	2.00	2.00	2.00
$\varepsilon_0/2$	3.90E−1	**6.63E−3**	1.77E−4	2.77E−6	4.32E−8
Order	–	**1.96**	1.74	2.00	2.00
$\varepsilon_0/2^2$	1.79	2.27E−1	**3.55E−3**	1.56E−5	2.44E−7
Order	–	0.99	**2.00**	2.61	2.00
$\varepsilon_0/2^3$	3.10	4.69E−1	2.06E−1	**3.22E−3**	5.03E−5
Order	–	0.91	0.40	**2.00**	2.00
$\varepsilon_0/2^4$	2.34	1.83	8.05E−1	2.04E−1	**3.19E−3**
Order	–	0.12	0.39	0.66	**2.00**

Table 5 Spatial and temporal error analysis of the sEWI-FP method for the Dirac equation (1.21) in 1D

Spatial errors	h_0=2	$h_0/2$	$h_0/2^2$	$h_0/2^3$	$h_0/2^4$
$\varepsilon_0 = 1$	8.79E−1	3.07E−1	3.73E−2	4.35E−5	4.12E−10
Order	–	1.52	3.04	9.74	16.69
$\varepsilon_0/2$	7.68E−1	1.89E−1	4.36E−3	3.83E−6	4.17E−10
Order	–	2.02	5.44	10.15	13.17
$\varepsilon_0/2^2$	6.35E−1	1.23E−1	1.28E−3	8.18E−7	3.98E−10
Order	–	2.37	6.59	10.61	11.01
$\varepsilon_0/2^3$	6.39E−1	1.17E−1	8.12E−4	3.62E−7	3.87E−10
Order	–	2.45	7.17	11.13	9.87
$\varepsilon_0/2^4$	6.28E−1	1.18E−1	7.36E−4	2.82E−7	6.18E−9
Order	–	2.41	7.32	11.35	5.51
$\varepsilon_0 = 1$	6.02E−2	**2.76E−3**	1.72E−4	1.07E−5	6.71E−7
Order	–	**2.22**	2.00	2.00	2.00

Table 5 continued

Temporal errors	τ_0=0.1	$\tau_0/4$	$\tau_0/4^2$	$\tau_0/4^3$	$\tau_0/4^4$
$\varepsilon_0/2$	9.33	9.16E−3	**5.66E−4**	3.53E−5	2.21E−6
Order	–	5.00	**2.01**	2.00	2.00
$\varepsilon_0/2^2$	Unstable	14.68	4.38E−3	**2.72E−4**	1.70E−5
Order	–	–	5.86	**2.00**	2.00
$\varepsilon_0/2^3$	8.77E−1	Unstable	Unstable	3.47E−3	**2.16E−4**
Order	–	–	–	–	**2.00**
$\varepsilon_0/2^4$	8.45E−1	8.47E−1	Unstable	5.46E−2	3.21E−3
Order	–	0.00	–	–	2.04

Table 6 Spatial and temporal error analysis of the TSFP method for the Dirac equation (1.21) in 1D

Spatial error	$h_0 = 2$	$h_0/2$	$h_0/2^2$	$h_0/2^3$	$h_0/2^4$
$\varepsilon_0 = 1$	1.10	2.43E−1	2.99E−3	2.79E−6	9.45E−9
Order	–	2.17	6.34	10.07	8.21
$\varepsilon_0/2$	1.06	1.46E−1	1.34E−3	9.61E−7	5.57E−9
Order	–	2.86	6.77	10.45	7.43
$\varepsilon_0/2^2$	1.11	1.43E−1	9.40E−4	5.10E−7	6.50E−9
Order	–	2.96	7.25	10.85	6.29
$\varepsilon_0/2^3$	1.15	1.44E−1	7.89E−4	3.62E−7	6.84E−9
Order	–	3.00	7.51	11.09	5.73
$\varepsilon_0/2^4$	1.18	1.45E−1	7.62E−4	2.88E−7	7.49E−9
Order	–	3.02	7.57	11.37	5.27
$\varepsilon_0/2^5$	1.19	1.46E−1	7.53E−4	2.59E−7	7.96E−9
Order	–	3.03	7.60	11.51	5.02
$\varepsilon_0/2^6$	1.20	1.47E−1	7.49E−4	2.63E−7	6.90E−9
Order	–	3.03	7.62	11.48	5.25

Temporal error	τ_0=0.4	$\tau_0/4$	$\tau_0/4^2$	$\tau_0/4^3$	$\tau_0/4^4$	$\tau_0/4^5$	$\tau_0/4^6$
$\varepsilon_0 = 1$	**2.17E−1**	1.32E−2	8.22E−4	5.13E−5	3.21E−6	2.01E−7	1.26E−8
Order	–	2.02	2.00	2.00	2.00	2.00	2.00
$\varepsilon_0/2$	1.32	**6.60E−2**	4.07E−3	2.54E−4	1.59E−5	9.92E−7	6.20E−8
Order	–	**2.16**	2.00	2.00	2.00	2.00	2.00
$\varepsilon_0/2^2$	2.50	3.33E−1	**1.68E−2**	1.04E−3	6.49E−5	4.06E−6	2.54E−7
Order	–	1.45	**2.15**	2.00	2.00	2.00	2.00
$\varepsilon_0/2^3$	1.79	1.97	8.15E−2	**4.15E−3**	2.57E−4	1.60E−5	1.00E−6
Order	–	-0.07	2.30	**2.14**	2.01	2.00	2.00
$\varepsilon_0/2^4$	1.35	8.27E−1	8.85E−1	2.01E−2	**1.03E−3**	6.35E−5	3.97E−6
Order	–	0.35	−0.05	2.73	**2.14**	2.01	2.00
$\varepsilon_0/2^5$	8.73E−1	2.25E−1	2.33E−1	2.49E−1	4.98E−3	**2.55E−4**	1.58E−5
Order	–	0.98	−0.03	−0.05	2.82	**2.14**	2.01

Table 7 Comparison of temporal errors of different methods for the Dirac equation (1.21) with $\varepsilon = 1$

$\varepsilon = 1$	τ_0=0.1	$\tau_0/4$	$\tau_0/4^2$	$\tau_0/4^3$	$\tau_0/4^4$	$\tau_0/4^5$
LFFD	1.38E−1	8.00E−3	4.98E−4	3.11E−5	1.94E−6	1.21E−7
Order	–	2.05	2.00	2.00	2.00	2.00
SIFD1	1.44E−1	8.85E−3	5.53E−4	3.27E−5	2.16E−6	1.35E−7
Order	–	2.01	2.00	2.04	1.96	2.00
SIFD2	1.72E−1	1.17E−2	7.30E−4	4.05E−5	2.85E−6	1.78E−7
Order	–	1.94	2.00	2.09	1.91	2.00
CNFD	5.48E−2	3.49E−3	2.18E−4	1.34E−5	8.38E−7	5.23E−8
Order	–	1.99	2.00	2.01	2.00	2.00
sEWI-FP	6.02E−2	2.76E−3	1.72E−4	1.07E−5	6.71E−7	4.19E−8
Order	–	2.22	2.00	2.00	2.00	2.00
TSFP	1.32E−2	8.22E−4	5.13E−5	3.21E−6	2.01E−7	1.26E−8
Order	–	2.00	2.00	2.00	2.00	2.00

Table 8 Comparison of temporal errors of different numerical methods for the Dirac equation (1.21) under proper ε-scalability

$\tau = O(\varepsilon^3)$ $h = O(\varepsilon)$	$\varepsilon_0 = 1$ $h_0 = 1/8$ $\tau_0 = 0.1$	$\varepsilon_0/2$ $h_0/2$ $\tau_0/8$	$\varepsilon_0/2^2$ $h_0/2^2$ $\tau_0/8^2$	$\varepsilon_0/2^3$ $h_0/2^3$ $\tau_0/8^3$	$\varepsilon_0/2^4$ $h_0/2^4$ $\tau_0/8^4$
LFFD	1.38E−1	1.14E−2	7.01E−3	6.42E−3	6.00E−3
SIFD1	1.44E−1	2.99E−2	1.54E−2	1.31E−2	1.26E−2
$\tau = O(\varepsilon^3)$	$\varepsilon_0 = 1$ $\tau_0 = 0.1$	$\varepsilon_0/2$ $\tau_0/8$	$\varepsilon_0/2^2$ $\tau_0/8^2$	$\varepsilon_0/2^3$ $\tau_0/8^3$	$\varepsilon_0/2^4$ $\tau_0/8^4$
SIFD2	1.72E−1	3.57E−2	1.63E−2	1.37E−2	1.28E−2
CNFD	5.48E−2	6.63E−3	3.55E−3	3.22E−3	3.19E−3
$\tau = O(\varepsilon^2)$	$\varepsilon_0 = 1$ $\tau_0 = 0.1$	$\varepsilon_0/2$ $\tau_0/4$	$\varepsilon_0/2^2$ $\tau_0/4^2$	$\varepsilon_0/2^3$ $\tau_0/4^3$	$\varepsilon_0/2^4$ $\tau_0/4^4$
sEWI-FP	6.02E−2	9.16E−3	4.38E−3	3.47E−3	3.21E−3
TSFP	1.32E−2	4.07E−3	1.04E−3	2.57E−4	6.35E−5

the 'correct' ε-scalability is $\tau = O(\varepsilon^3)$ which verifies our theoretical results; for the sEWI-FP and TSFP methods, the 'correct' ε-scalability is $\tau = O(\varepsilon^2)$ which again confirms our theoretical results. In fact, for $0 < \varepsilon \leq 1$, one can observe clearly second-order convergence in time for the FDTD methods only when $\tau \lesssim \varepsilon^3$ (cf. upper triangles above the diagonal labelled by bold letters in the lower parts of Tables 1, 2, 3, 4), and resp., for the sEWI-FP and TSFP methods when $\tau \lesssim \varepsilon^2$ (cf. upper triangles above the diagonal labelled by bold letters in the lower parts of Tables 5 and 6). In general, for any fixed $0 < \varepsilon \leq 1$ and $\tau > 0$, the TSFP method performs the best, and the sEWI-FP method performs much better than the FDTD methods in temporal discretization (cf. Table 8).

Table 9 Spatial error analysis of the CNFD method for the free Dirac equation with different h

ε	$\varepsilon_0 = 1$	$\varepsilon_0/2$	$\varepsilon_0/2^2$	$\varepsilon_0/2^3$	$\varepsilon_0/2^4$
$h_0 = 1/256$	1.61E−1	3.21E−1	6.35E−1	1.21	2.07
$h_0/2$	4.03E−2	8.05E−2	1.59E−1	3.07E−1	5.43E−1
$h_0/2^2$	1.01E−2	2.01E−2	3.99E−2	7.69E−2	1.36E−1
$h_0/2^3$	2.52E−3	5.03E−3	9.97E−3	1.92E−2	3.41E−2
$h_0/2^4$	6.30E−4	1.26E−3	2.47E−3	4.95E−3	8.64E−3

(iii). From Table 6, our numerical results suggest the following error bound for the TSFP method when $\tau \lesssim \varepsilon^2$,

$$\|\Phi(t_n, \cdot) - I_M(\Phi^n)\|_{L^2} \lesssim h^{m_0} + \frac{\tau^2}{\varepsilon^2}, \quad 0 \le n \le \frac{T}{\tau}, \tag{5.3}$$

which is much better than (4.7) for the TSFP method in the nonrelativistic limit regime. Rigorous mathematical justification for (5.3) is on-going.

From Tables 1, 2, 3, and 4, in the numerical example, we could not observe numerically the ε-dependence in the spatial discretization error for the FDTD methods, i.e. $\frac{1}{\varepsilon}$ in front of h^2, which was proven in Theorems 2.2–2.4. In order to investigate the spatial ε-resolution of the FDTD methods, we consider the Dirac equation (2.1) on $\Omega = (-1, 1)$ with no electromagnetic potential—the free Dirac equation, i.e.

$$A_1(t, x) \equiv 0, \quad V(t, x) \equiv 0, \quad x \in (-1, 1), \quad t \ge 0. \tag{5.4}$$

The initial data in (2.2) is taken as

$$\phi_1(0, x) = e^{9\pi i(x+1)}, \quad \phi_2(0, x) = e^{9\pi i(x+1)}, \quad -1 \le x \le 1. \tag{5.5}$$

Table 9 shows the spatial errors $e_{h,\tau_e}(t = 2)$ of the CNFD method with different h. The results for the LFFD, SIFD1 and SIFD2 methods are similar and they are omitted here for brevity. From Table 9 where the error is of order h^2/ε (each row of the table), we can conclude that the error bounds in the Theorems 2.1–2.4 are sharp.

Based on the above comparison, in view of both temporal and spatial accuracies and resolution capacity, we conclude that the sEWI-FP and TSFP methods perform much better than the FDTD methods for the discretization of the Dirac equation, especially in the nonrelativistic limit regime. For the reader's convenience, we summarize the properties of different numerical methods in Table 10.

As observed in [15,16], the time-splitting spectral (TSSP) method for the Schrödinger equation performs much better for the physical observable, e.g. density and current, than for the wave function, in the semiclassical limit regime with respect to the scaled Planck constnat $0 < \varepsilon \ll 1$. In order to see whether this is still valid for the TSFP method for the Dirac equation in the nonrelativistic limit regime, let $\rho^n = |\Phi^n_{h,\tau}|^2$, $\mathbf{J}^n = \frac{1}{\varepsilon}(\Phi^n_{h,\tau})^* \sigma_1 \Phi^n_{h,\tau}$ with $\Phi^n_{h,\tau}$ the numerical solution obtained by the TSFP method with mesh size h and time step τ, and define the errors

Table 10 Comparison of properties of different numerical methods for solving the Dirac equation with M being the number of grid points in space

Method	LFFD	SIFD1	CNFD	sEWI-FP	TSFP
Time symmetric	Yes	Yes	Yes	Yes	Yes
Mass conservation	No	No	Yes	No	Yes
Energy conservation	No	No	Yes	No	No
Dispersion relation	No	No	No	No	Yes
Unconditionally stable	No	No	Yes	No	Yes
Explicit scheme	Yes	No	No	Yes	Yes
Temporal accuracy	2nd	2nd	2nd	2nd	2nd
Spatial accuracy	2nd	2nd	2nd	Spectral	Spectral
Memory cost	$O(M)$	$O(M)$	$O(M)$	$O(M)$	$O(M)$
Computational cost	$O(M)$	$O(M \ln M)$	$\gg O(M)$	$O(M \ln M)$	$O(M \ln M)$
Resolution when $0 < \varepsilon \ll 1$	$h = O(\sqrt{\varepsilon})$ $\tau = O(\varepsilon^3)$	$h = O(\sqrt{\varepsilon})$ $\tau = O(\varepsilon^3)$	$h = O(\sqrt{\varepsilon})$ $\tau = O(\varepsilon^3)$	$h = O(1)$ $\tau = O(\varepsilon^2)$	$h = O(1)$ $\tau = O(\varepsilon^2)$

SIFD2 is the same as SIFD1 and is omitted

$$e_\rho^{h,\tau}(t_n) := \|\rho^n - \rho(t_n,\cdot)\|_{l^1} = h\sum_{j=0}^{N-1} |\rho_j^n - \rho(t_n, x_j)|,$$
$$e_{\mathbf{J}}^{h,\tau}(t_n) := \|\mathbf{J}^n - \mathbf{J}(t_n,\cdot)\|_{l^1} = h\sum_{j=0}^{N-1} |\mathbf{J}_j^n - \mathbf{J}(t_n, x_j)|.$$

Table 11 lists temporal errors $e_\rho^{h,\tau}(t = 2)$ and $e_{\mathbf{J}}^{h,\tau}(t = 2)$ with different τ for the TSFP method (4.4). From this Table, we can see that the approximations of the density and current are at the same order as for the wave function by using the TSFP method. The reason that we can speculate is that $\rho = O(1)$ and $\mathbf{J} = O(\varepsilon^{-1})$ (see details in Eqs. 1.11 or 1.23) in the Dirac equation, where in the Schrödinger equation both density and current are all at $O(1)$, when $0 < \varepsilon \ll 1$.

5.2 Dynamics of the Dirac Equation in 2D

Here we study numerically the dynamics of the Dirac equation (1.21) in 2D with a honeycomb lattice potential, i.e. we take $d = 2$, $A_1(t, \mathbf{x}) = A_2(t, \mathbf{x}) \equiv 0$ and

$$V(t, \mathbf{x}) = \cos\left(\frac{4\pi}{\sqrt{3}}\mathbf{e}_1 \cdot \mathbf{x}\right) + \cos\left(\frac{4\pi}{\sqrt{3}}\mathbf{e}_2 \cdot \mathbf{x}\right) + \cos\left(\frac{4\pi}{\sqrt{3}}\mathbf{e}_3 \cdot \mathbf{x}\right), \tag{5.6}$$

with

$$\mathbf{e}_1 = (-1, 0)^T, \quad \mathbf{e}_2 = (1/2, \sqrt{3}/2)^T, \quad \mathbf{e}_3 = (1/2, -\sqrt{3}/2)^T. \tag{5.7}$$

The initial data in (1.22) is taken as

$$\phi_1(0, \mathbf{x}) = e^{-\frac{x^2+y^2}{2}}, \quad \phi_2(0, \mathbf{x}) = e^{-\frac{(x-1)^2+y^2}{2}}, \quad \mathbf{x} = (x, y)^T \in \mathbb{R}^2. \tag{5.8}$$

The problem is solved numerically on $\Omega = [-10, 10]^2$ by the TSFP method with mesh size $h = 1/16$ and time step $\tau = 0.01$. Figures 2 and 3 depict the densities $\rho_j(t, \mathbf{x}) = |\phi_j(t, \mathbf{x})|^2$ $(j = 1, 2)$ for $\varepsilon = 1$ and $\varepsilon = 0.2$, respectively.

Table 11 Temporal errors for density and current of the TSFP for the Dirac equation (1.21) in 1D

$e_\rho^{h,\tau}(t=2)$	τ_0=0.4	$\tau_0/4$	$\tau_0/4^2$	$\tau_0/4^3$	$\tau_0/4^4$	$\tau_0/4^5$	$\tau_0/4^6$
$\varepsilon_0=1$	**2.50E−1**	1.54E−2	9.61E−4	6.01E−5	3.75E−6	2.34E−7	1.43E−8
Order	–	2.01	2.00	2.00	2.00	2.00	2.01
$\varepsilon_0/2$	1.22	**5.27E−2**	3.21E−3	2.01E−4	1.25E−5	7.84E−7	4.92E−8
Order	–	**2.27**	2.02	2.00	2.00	2.00	2.01
$\varepsilon_0/2^2$	1.75	1.86E−1	**1.00E−2**	6.20E−4	3.87E−5	2.42E−6	1.52E−7
Order	–	1.62	**2.11**	2.01	2.00	2.00	2.00
$\varepsilon_0/2^3$	1.11	1.39	2.95E−2	**1.53E−3**	9.47E−5	5.92E−6	3.72E−7
Order	–	−0.16	2.78	**2.13**	2.01	2.00	2.00
$\varepsilon_0/2^4$	1.58	7.58E−1	7.81E−1	5.46E−3	**3.01E−4**	1.87E−5	1.17E−6
Order	–	0.53	-0.02	3.58	**2.09**	2.00	2.00
$\varepsilon_0/2^5$	9.59E−1	1.96E−1	2.29E−1	2.33E−1	1.20E−3	**6.76E−5**	4.21E−6
Order	–	1.15	−0.11	−0.01	3.8	**2.07**	2.00
$e_{\mathbf{J}}^{h,\tau}(t=2)$	τ_0=0.4	$\tau_0/4$	$\tau_0/4^2$	$\tau_0/4^3$	$\tau_0/4^4$	$\tau_0/4^5$	$\tau_0/4^6$
$\varepsilon_0=1$	**1.70E−1**	1.09E−2	6.83E−4	4.27E−5	2.67E−6	1.67E−7	1.02E−8
Order	–	1.98	2.00	2.00	2.00	2.00	2.01
$\varepsilon_0/2$	9.15E−1	**6.39E−2**	4.00E−3	2.50E−4	1.56E−5	9.76E−7	6.08E−8
Order	–	**1.92**	2.00	2.00	2.00	2.00	2.00
$\varepsilon_0/2^2$	1.58	3.45E−1	**1.69E−2**	1.04E−3	6.50E−5	4.06E−6	2.54E−7
Order	–	1.10	**2.18**	2.01	2.00	2.00	2.00
$\varepsilon_0/2^3$	1.06	1.26	5.83E−2	**2.87E−3**	1.76E−4	1.11E−5	6.94E−7
Order	–	−0.12	2.22	**2.17**	2.01	2.00	2.00
$\varepsilon_0/2^4$	1.11	9.78E−1	1.05	2.28E−2	**1.18E−3**	7.33E−5	4.58E−6
Order	–	0.09	−0.05	2.76	**2.13**	2.00	2.00
$\varepsilon_0/2^5$	4.98E−1	1.55E−1	2.22E−1	2.39E−1	4.04E−3	**2.09E−4**	1.29E−5
Order	–	0.84	−0.30	−0.05	2.94	**2.13**	2.01

From Figs. 2 and 3, we find that the dynamics of the Dirac equation depends significantly on ε. For $\varepsilon = 1$, the dynamics is strange and the densities are fluctuating in a random pattern, featured as quantum Zitterbewegung [30], well-known for the relativistic Dirac dynamics. As $\varepsilon \to 0^+$, the relativistic effects will vanish and the Dirac equation will reduce to Schrödinger equations. Indeed, from Fig. 3 where $\varepsilon = 0.2$, we find the dynamics is more like Schrödinger dynamics and the densities spread over the lattice potential in a smoother way. In addition, the TSFP method can capture the dynamics very accurately and efficiently.

6 Conclusion

Three types of numerical methods based on different time integrations were analyzed rigorously and compared numerically for simulating the Dirac equation in the nonrelativistic limit regime, i.e. $0 < \varepsilon \ll 1$ or the speed of light goes to infinity. The first class consists of the

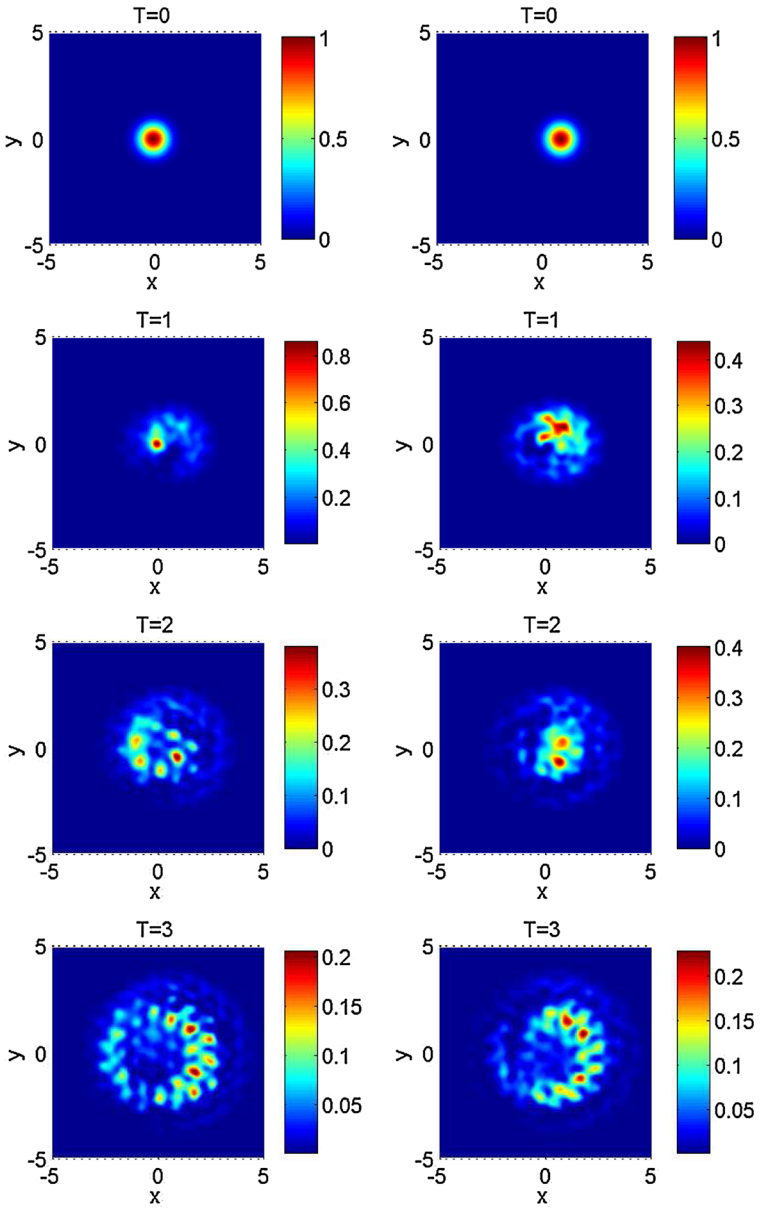

Fig. 2 Dynamics of the densities $\rho_1(t,\mathbf{x}) = |\phi_1(t,\mathbf{x})|^2$ (*left*) and $\rho_2(t,\mathbf{x}) = |\phi_2(t,\mathbf{x})|^2$ (*right*) of the Dirac equation in 2D with a honeycomb lattice potential when $\varepsilon = 1$

second order standard FDTD methods, including energy conservative/ nonconservative and implicit/semi-implicit/explicit ones. In the nonrelativistic limit regime, the error estimates of the FDTD methods were rigorously analyzed, which suggest that the ε-scalability of the FDTD methods is $\tau = O(\varepsilon^3)$ and $h = O(\sqrt{\varepsilon})$. The second class applies the Fourier spectral discretization in space and Gautschi-type integration in time, resulting in an sEWI-FP

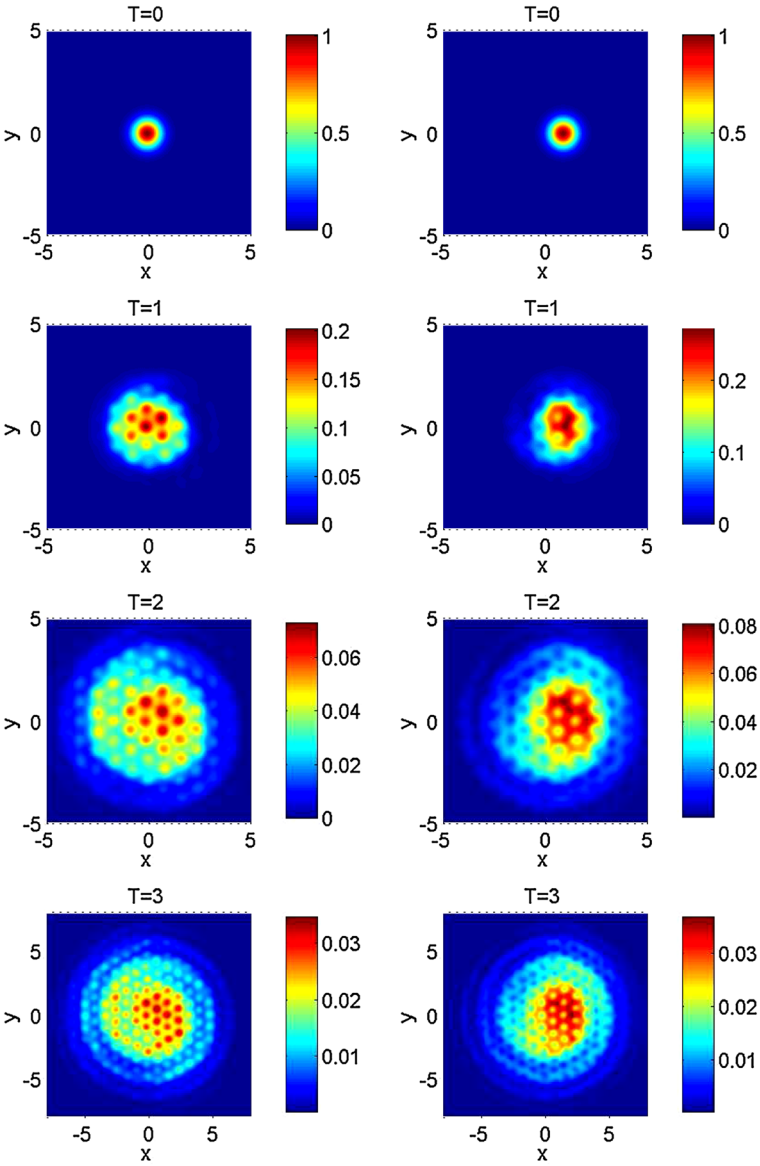

Fig. 3 Dynamics of the densities $\rho_1(t,\mathbf{x}) = |\phi_1(t,\mathbf{x})|^2$ (*left*) and $\rho_2(t,\mathbf{x}) = |\phi_2(t,\mathbf{x})|^2$ (*right*) of the Dirac equation in 2D with a honeycomb potential when $\varepsilon = 0.2$

method. Rigorous error bounds for the sEWI-FP method were derived, which show that the ε-scalability of the sEWI-FP method is $\tau = O(\varepsilon^2)$ and $h = O(1)$. The last class combines the Fourier spectral discretization in space and splitting technique in time, which leads to a TSFP method. Based on the rigorous error analysis, the ε-scalability of the TSFP method is $\tau = O(\varepsilon^2)$ and $h = O(1)$, which is similar to the sEWI-FP method. From the error analysis and numerical results, the sEWI-FP and TSFP methods perform much better than the FDTD methods, especially in the nonrelativistic limit regime. Extensive numerical results indicate

that the TSFP method is superior than the sEWI-FP in terms of accuracy and efficiency, and thus the TSFP method is favorable for solving the Dirac equation directly, especially in the nonrelativistic limit regime. Finally, we studied the dynamics of the Dirac equation in 2D with a honeycomb lattice potential and observed some interesting dynamics for different ε.

Acknowledgements Part of this work was done when the authors were visiting the Institute for Mathematical Sciences at the National University of Singapore in 2015.

Appendix 1

Proof of Theorem 2.1 for the LFFD method

Define the local truncation error $\tilde{\xi}^n = (\tilde{\xi}_0^n, \tilde{\xi}_1^n, \ldots, \tilde{\xi}_M^n)^T \in X_M$ of the LFFD (2.6) with (2.10) and (2.11) as follows, for $0 \le j \le M-1$ and $n \ge 1$,

$$\tilde{\xi}_j^n := \left[i\delta_t \Phi + \frac{i}{\varepsilon}\sigma_1 \delta_x \Phi - \frac{1}{\varepsilon^2}\sigma_3 \Phi + \left(A_{1,j}^n \sigma_1 - V_j^n I_2 \right) \Phi \right]_{t=t_n, x=x_j}, \tag{6.1}$$

$$\tilde{\xi}_j^0 := i\delta_t^+ \Phi(0, x_j) + \frac{i}{\varepsilon}\sigma_1 \delta_x \Phi_0(x_j) - \left(\frac{1}{\varepsilon^2}\sigma_3 + V_j^0 I_2 - A_{1,j}^0 \sigma_1 \right) \Phi_0(x_j). \tag{6.2}$$

Applying the Taylor expansion in (6.1) and (6.2) we obtain for $j = 0, 1, \ldots, M-1$ and $n \ge 1$,

$$\tilde{\xi}_j^0 = i\tau \partial_{tt} \Phi(\tau', x_j) + \frac{i}{\varepsilon} h^2 \partial_{xxx} \Phi_0(x'), \quad \tilde{\xi}_j^n = i\tau^2 \partial_{ttt} \Phi(t', x_j) + \frac{i}{\varepsilon} h^2 \partial_{xxx} \Phi(t_n, x''),$$

where $t' \in (0, \tau)$, $t'' \in (t_{n-1}, t_{n+1})$, $x', x'' \in (x_{j-1}, x_{j+1})$. Noticing (2.1) and the assumptions (A) and (B), we have

$$|\tilde{\xi}_j^0| \lesssim \frac{\tau}{\varepsilon^4} + \frac{h^2}{\varepsilon}, \quad |\tilde{\xi}_j^n| \lesssim \frac{\tau^2}{\varepsilon^6} + \frac{h^2}{\varepsilon}, \quad j = 0, 1, \ldots, M-1, \quad n \ge 1, \tag{6.3}$$

which immediately implies

$$\|\tilde{\xi}^n\|_{l^\infty} = \max_{0 \le j \le M-1} |\tilde{\xi}_j^n| \lesssim \frac{\tau^2}{\varepsilon^6} + \frac{h^2}{\varepsilon}, \ \|\tilde{\xi}^n\|_{l^2} \lesssim \|\tilde{\xi}^n\|_{l^\infty} \lesssim \frac{\tau^2}{\varepsilon^6} + \frac{h^2}{\varepsilon}, \ n \ge 1. \tag{6.4}$$

Subtracting (2.6) from (6.1), noticing (2.32), we get for $0 \le j \le M-1$ and $n \ge 1$,

$$i\delta_t \mathbf{e}_j^n = -\frac{i}{\varepsilon}\sigma_1 \delta_x \mathbf{e}_j^n + \frac{1}{\varepsilon^2}\sigma_3 \mathbf{e}_j^n + \left(V_j^n I_2 - A_{1,j}^n \sigma_1 \right) \mathbf{e}_j^n + \tilde{\xi}_j^n, \tag{6.5}$$

where the boundary and initial conditions are given as

$$\mathbf{e}_0^n = \mathbf{e}_M^n, \quad \mathbf{e}_{-1}^n = \mathbf{e}_{M-1}^n, \quad n \ge 0, \quad \mathbf{e}_j^0 = \mathbf{0}, \quad j = 0, 1, \ldots, M. \tag{6.6}$$

For the first step, we have

$$\|\mathbf{e}^1\|_{l^2} = \tau \|\tilde{\xi}^0\|_{l^2} \lesssim \frac{\tau^2}{\varepsilon^4} + \frac{\tau h^2}{\varepsilon} \lesssim \frac{h^2}{\varepsilon} + \frac{\tau^2}{\varepsilon^6}. \tag{6.7}$$

Denote $\mathcal{E}^{n+1}$ for $n = 0, 1, \ldots$ as

$$\mathcal{E}^{n+1} = \|\mathbf{e}^{n+1}\|_{l^2}^2 + \|\mathbf{e}^{n}\|_{l^2}^2 + 2\,\mathrm{Re}\left(\tau h \sum_{j=0}^{M-1} (\mathbf{e}_j^{n+1})^* \sigma_1 \delta_x \mathbf{e}_j^n\right) - 2\,\mathrm{Im}\left(\frac{\tau h}{\varepsilon^2} \sum_{j=0}^{M-1} (\mathbf{e}_j^{n+1})^* \sigma_3 \mathbf{e}_j^n\right); \tag{6.8}$$

and under the stability condition (2.33), e.g., $\tau \le \frac{\varepsilon^2 \tau_1 h}{\varepsilon^2 h V_{\max} + \sqrt{h^2 + \varepsilon^2 (1 + \varepsilon h A_{1,\max})^2}}$ with $\tau_1 = \frac{1}{4}$, which implies $\frac{\tau}{h} \le \frac{1}{4}$ and $\frac{\tau}{\varepsilon^2} \le \frac{1}{4}$, using Cauchy inequality, we can get that

$$\frac{1}{2}\left(\|\mathbf{e}^{n+1}\|_{l^2}^2 + \|\mathbf{e}^{n}\|_{l^2}^2\right) \le \mathcal{E}^{n+1} \le \frac{3}{2}\left(\|\mathbf{e}^{n+1}\|_{l^2}^2 + \|\mathbf{e}^{n}\|_{l^2}^2\right), \quad n \ge 0. \tag{6.9}$$

It follows from (6.7) that

$$\mathcal{E}^1 \lesssim \left(\frac{h^2}{\varepsilon} + \frac{\tau^2}{\varepsilon^6}\right)^2. \tag{6.10}$$

Multiplying (6.5) from the left by $2h\tau(\mathbf{e}_j^{n+1} + \mathbf{e}_j^{n-1})^*$, taking the imaginary part, then summing for $j = 0, 1, \ldots, M-1$, using Cauchy inequality, noting (6.4) and (6.9), we get for $n \ge 1$,

$$\begin{aligned}\mathcal{E}^{n+1} - \mathcal{E}^n \lesssim & h\tau \sum_{j=0}^{M-1} \left((A_{1,\max} + V_{\max})|\mathbf{e}_j^n| + |\tilde{\xi}_j^n|\right)\left(|\mathbf{e}_j^{n+1}| + |\mathbf{e}_j^{n-1}|\right) \\ \lesssim & \tau(\mathcal{E}^{n+1} + \mathcal{E}^n) + \tau\left(\frac{h^2}{\varepsilon} + \frac{\tau^2}{\varepsilon^6}\right)^2, \quad n \ge 0.\end{aligned}$$

Summing the above inequality for $n = 1, 2, \ldots, m-1$, we get

$$\mathcal{E}^m - \mathcal{E}^1 \lesssim \tau \sum_{k=1}^{m} \mathcal{E}^k + m\tau\left(\frac{h^2}{\varepsilon} + \frac{\tau^2}{\varepsilon^6}\right)^2, \quad 1 \le m \le \frac{T}{\tau}. \tag{6.11}$$

Taking τ_0 sufficiently small, using the discrete Gronwall's inequality and noticing (6.10), we obtain from the above equation that

$$\mathcal{E}^m \lesssim \left(\frac{h^2}{\varepsilon} + \frac{\tau^2}{\varepsilon^6}\right)^2, \quad 1 \le m \le \frac{T}{\tau}, \tag{6.12}$$

which immediately implies the error bound (2.34) in view of (6.9). □

Appendix 2

Proof of Theorem 3.1 for the sEWI-FP method

Define the error function $\mathbf{e}^n(x)$ for $n = 0, 1, \ldots$ as

$$\mathbf{e}^n(x) = \begin{pmatrix} e_1^n(x) \\ e_2^n(x) \end{pmatrix} := P_M \Phi(t_n, x) - \Phi_M^n(x) = \sum_{l=-M/2}^{M/2-1} \widehat{\mathbf{e}}_l^n e^{i\mu_l(x-a)}, \ a \le x \le b. \tag{6.13}$$

Using the triangular inequality and standard interpolation result, we get

$$\begin{aligned}\|\Phi(t_n,x)-\Phi_M^n(x)\|_{L^2} &\le \|\Phi(t_n,x)-P_M\Phi(t_n,x)\|_{L^2}+\|\mathbf{e}^n(x)\|_{L^2}\\ &\le h^{m_0}+\|\mathbf{e}^n(x)\|_{L^2},\end{aligned}\tag{6.14}$$

where $0\le n\le \frac{T}{\tau}$, and the above result means that we only need estimate $\|\mathbf{e}^n(x)\|_{L^2}$.

Define the local truncation error $\xi^n(x)=\sum_{l=-M/2}^{M/2-1}\widehat{\xi}_l^n e^{i\mu_l(x-a)}\in Y_M$ of the sEWI-FP (3.17) for $n\ge 1$ as

$$\widehat{\xi}_l^n=(\widehat{\Phi(t_{n+1})})_l+2i\sin(\frac{\tau\Gamma_l}{\varepsilon^2})\,(\widehat{\Phi(t_n)})_l-(\widehat{\Phi(t_{n-1})}_l+2i\frac{\varepsilon^2}{\delta_l}\sin(\frac{\tau\delta_l}{\varepsilon^2})(G\widehat{(t_n)\Phi(t_n)})_l,\tag{6.15}$$

and for $n=0$ as

$$\widehat{\xi}_l^0=(\widehat{\Phi(\tau)})_l-e^{-i\tau\Gamma_l/\varepsilon^2}\,(\widehat{\Phi(0)})_l+\varepsilon^2\Gamma_l^{-1}\left[I_2-e^{-\frac{i\tau}{\varepsilon^2}\Gamma_l}\right](G\widehat{(0)\Phi(0)})_l,\tag{6.16}$$

where we write $\Phi(t)$ and $G(t)$ in short for $\Phi(t,x)$ and $G(t,x)$, respectively.

Firstly, we estimate the local truncation error $\xi^n(x)$. Multiplying both sides of the Dirac equation (2.1) by $e^{i\mu_l(x-a)}$ and integrating over the interval (a,b), we easily recover the equations for $(\widehat{\Phi(t)})_l$, which are exactly the same as (3.6) with Φ_M being replaced by $\Phi(t,x)$. Replacing Φ_M with $\Phi(t,x)$, we use the same notations $\widehat{F}_l^n(s)$ as in (3.7) and the time derivatives of $\widehat{F}_l^n(s)$ enjoy the same properties of time derivatives of $\Phi(t,x)$. Thus, the same representation (3.12) holds for $(\widehat{\Phi(t_n)})_l$ with $n\ge 1$. From the derivation of the EWI method, it is clear that the error $\xi^n(x)$ comes from the approximations for the integrals in (3.13) and (3.14), and we have

$$\widehat{\xi}_l^0=-i\int_0^\tau e^{\frac{i(s-\tau)}{\varepsilon^2}\Gamma_l}(\widehat{F}_l^0(s)-\widehat{F}_l^0(0))ds=-i\int_0^\tau\int_0^s e^{\frac{i(s-\tau)}{\varepsilon^2}\Gamma_l}\partial_{s_1}\widehat{F}_l^0(s_1)\,ds_1ds,$$

and for $n\ge 1$

$$\begin{aligned}\widehat{\xi}_l^n=&-i\int_0^\tau\cos((s-\tau)\delta_l/\varepsilon^2)\int_0^s\int_{-s_1}^{s_1}\partial_{s_2s_2}\widehat{F}_l^n(s_2)\,ds_2ds_1ds\\ &+\int_0^\tau\sin\left(\frac{(s-\tau)\Gamma_l}{\varepsilon^2}\right)\int_{-s}^s\partial_{s_1}\widehat{F}_l^n(s_1)\,ds_1\,ds.\end{aligned}\tag{6.17}$$

For $n=0$, the above equalities imply $|\widehat{\xi}_l^0|\lesssim\int_0^\tau\int_0^s|\partial_{s_1}\widehat{F}_l^0(s_1)|ds_1ds$ and by the Bessel inequality and assumptions (C) and (D), we find

$$\begin{aligned}\|\xi^0(x)\|_{L^2}^2=&(b-a)\sum_{l=-M/2}^{M/2-1}|\widehat{\xi}_l^0|^2\lesssim(b-a)\tau^2\int_0^\tau\int_0^s\sum_{l=-M/2}^{M/2-1}|\partial_{s_1}\widehat{F}_l^0(s_1)|^2\,ds_1ds\\ \lesssim&\tau^2\int_0^\tau\int_0^s\|\partial_{s_1}(G(s_1)\Phi(s_1))\|_{L^2}^2\,ds_1ds\lesssim\frac{\tau^4}{\varepsilon^4}.\end{aligned}$$

Similarly, for $n \geq 1$, we obtain

$$\begin{aligned}
\|\xi^n(x)\|_{L^2}^2 &= (b-a)\sum_{l=-M/2}^{M/2-1} |\widehat{\xi}_l^n|^2 \\
&\lesssim \tau^3 \int_0^\tau \int_0^s \int_{-s_1}^{s_1} \sum_{l=-\frac{M}{2}}^{\frac{M}{2}-1} |\partial_{s_2 s_2} \widehat{F}_l^n(s_2)|^2 \, ds_2 ds_1 ds \\
&\quad + \tau^2 \int_0^\tau \int_{-s}^{s} \frac{(\tau-s)^2}{\varepsilon^4} \sum_{l=-\frac{M}{2}}^{\frac{M}{2}-1} |\partial_{\theta_1} \widehat{F}_l^{n-1}(\theta_1)|^2 \, d\theta_1 \, d\theta \, ds \\
&\lesssim \tau^6 \|\partial_{tt}(G(t)\Phi(t))\|_{L^\infty([0,T];(L^2)^2)}^2 + \frac{\tau^6}{\varepsilon^4} \|\partial_t(G(t)\Phi(t))\|_{L^\infty([0,T];(L^2)^2)}^2 \lesssim \frac{\tau^6}{\varepsilon^8},
\end{aligned}$$

where we have used the assumptions (C) and (D). Hence, we derive that

$$\|\xi^0(x)\|_{L^2} \lesssim \frac{\tau^2}{\varepsilon^2}, \quad \|\xi^n(x)\|_{L^2} \lesssim \frac{\tau^3}{\varepsilon^4}, \quad n \geq 1. \tag{6.18}$$

Now, we look at the error equations. For each fixed $l = -M/2, \ldots, M/2-1$, subtracting (3.17) from (6.15), we obtain the equation for the error vector function as

$$\widehat{\mathbf{e}}_l^0 = \mathbf{0}, \quad \widehat{\mathbf{e}}_l^1 = \widehat{\xi}_l^0; \quad \widehat{\mathbf{e}}_l^{n+1} - \widehat{\mathbf{e}}_l^{n-1} = -2i \sin(\tau \Gamma_l/\varepsilon^2)\widehat{\mathbf{e}}_l^n + \widehat{R}_l^n + \widehat{\xi}_l^n, \tag{6.19}$$

where $1 \leq n \leq \frac{T}{\tau} - 1$, and $R^n(x) = \sum_{l=-M/2}^{M/2-1} \widehat{R}_l^n e^{i\mu_l(x-a)} \in Y_M$ for $n \geq 1$ is given by

$$\widehat{R}_l^n = 2i\varepsilon^2 \delta_l^{-1} \sin(\tau\delta_l/\varepsilon^2) \left(\widehat{(G(t_n)\Phi(t_n))}_l - \widehat{(G(t_n)\Phi_M^n)}_l \right). \tag{6.20}$$

Since $|\varepsilon^2 \delta_l^{-1} \sin(\tau\delta_l/\varepsilon^2)| \leq \tau$, from (6.20) and the assumption (D), we get

$$\begin{aligned}
\|R^n(x)\|_{L^2}^2 =& (b-a)\sum_{l=-M/2}^{M/2-1} |\widehat{R}_l^n|^2 \\
\lesssim& (b-a)\tau^2 \sum_{l=-M/2}^{M/2-1} \left| \widehat{(G(t_n)\Phi(t_n))}_l - \widehat{(G(t_n)\Phi_M^n)}_l \right|^2 \\
\lesssim& \tau^2 \|G(t_n)\Phi(t_n,x) - G(t_n)\Phi_M^n(x)\|_{L^2}^2 \lesssim \tau^2 \|\Phi(t_n,x) - \Phi_M^n(x)\|_{L^2}^2 \\
\lesssim& \tau^2 h^{2m_0} + \tau^2 \|\mathbf{e}^n(x)\|_{L^2}^2.
\end{aligned} \tag{6.21}$$

Multiplying both sides of (6.19) by $\left(\widehat{\mathbf{e}}_l^n\right)^*$ from left, taking the real parts, we obtain

$$\mathrm{Re}\left((\widehat{\mathbf{e}}_l^n)^* \widehat{\mathbf{e}}_l^{n+1} \right) - \mathrm{Re}\left((\widehat{\mathbf{e}}_l^n)^* \widehat{\mathbf{e}}_l^{n-1} \right) = \mathrm{Re}\left((\widehat{\mathbf{e}}_l^n)^* (\widehat{R}_l^n + \widehat{\xi}_l^n) \right),$$

which implies

$$\begin{aligned}
|\widehat{\mathbf{e}}_l^{n+1}|^2 + |\widehat{\mathbf{e}}_l^n|^2 - |\widehat{\mathbf{e}}_l^{n+1} - \widehat{\mathbf{e}}_l^n|^2 = |\widehat{\mathbf{e}}_l^n|^2 + |\widehat{\mathbf{e}}_l^{n-1}|^2 - |\widehat{\mathbf{e}}_l^n - \widehat{\mathbf{e}}_l^{n-1}|^2 \\
+2\,\mathrm{Re}\left((\widehat{\mathbf{e}}_l^n)^* (\widehat{R}_l^n + \widehat{\xi}_l^n) \right).
\end{aligned} \tag{6.22}$$

Multiplying both sides of (6.19) by $\left(\widehat{\mathbf{e}}_l^{n+1}-2\widehat{\mathbf{e}}_l^{n}+\widehat{\mathbf{e}}_l^{n-1}\right)^*$ from left, taking the real parts, we have

$$\begin{aligned}&\left|\widehat{\mathbf{e}}_l^{n+1}-\widehat{\mathbf{e}}_l^{n}\right|^2-\left|\widehat{\mathbf{e}}_l^{n}-\widehat{\mathbf{e}}_l^{n-1}\right|^2\\ =&2\,\mathrm{Im}\left((\widehat{\mathbf{e}}_l^{n+1})^*\sin(\tau\Gamma_l/\varepsilon^2)\widehat{\mathbf{e}}_l^{n}\right)-2\,\mathrm{Im}\left((\widehat{\mathbf{e}}_l^{n})^*\sin(\tau\Gamma_l/\varepsilon^2)\widehat{\mathbf{e}}_l^{n-1}\right)\\ &+\mathrm{Re}\left((\widehat{\mathbf{e}}_l^{n+1}-2\widehat{\mathbf{e}}_l^{n}+\widehat{\mathbf{e}}_l^{n-1})^*(\widehat{R}_l^{n}+\widehat{\xi}_l^{n})\right).\end{aligned}\tag{6.23}$$

Summing (6.22) and (6.23), then applying Cauchy inequality and triangle inequality, we get

$$\begin{aligned}&|\widehat{\mathbf{e}}_l^{n+1}|^2+|\widehat{\mathbf{e}}_l^{n}|^2-2\,\mathrm{Im}\left((\widehat{\mathbf{e}}_l^{n+1})^*\sin(\tau\Gamma_l/\varepsilon^2)\widehat{\mathbf{e}}_l^{n}\right)\\ \le&|\widehat{\mathbf{e}}_l^{n}|^2+|\widehat{\mathbf{e}}_l^{n-1}|^2-2\mathrm{Im}\left((\widehat{\mathbf{e}}_l^{n})^*\sin(\tau\Gamma_l/\varepsilon^2)\widehat{\mathbf{e}}_l^{n-1}\right)\\ &+\tau(|\widehat{\mathbf{e}}_l^{n+1}|^2+|\widehat{\mathbf{e}}_l^{n-1}|^2)+\frac{1}{\tau}(|\widehat{R}_l^{n}|^2+|\widehat{\xi}_l^{n}|^2).\end{aligned}\tag{6.24}$$

Denote

$$\mathcal{E}^n=\left\|\mathbf{e}^{n+1}(x)\right\|_{L^2}^2+\left\|\mathbf{e}^{n}(x)\right\|_{L^2}^2-2(b-a)\sum_{l=-M/2}^{M/2-1}\mathrm{Im}\left((\widehat{\mathbf{e}}_l^{n+1})^*\sin(\tau\Gamma_l/\varepsilon^2)\widehat{\mathbf{e}}_l^{n}\right),\tag{6.25}$$

and it follows from the stability constraint (3.25) that the matrix l^2 norm satisfies $\|\sin(\frac{\tau\Gamma_l}{\varepsilon^2})\|_{l^2}\le\sin(\tau\delta_l/\varepsilon^2)\le\sin(\pi/3)=\sqrt{3}/2$, which yield the following conclusion

$$\begin{aligned}\mathcal{E}^n\ge&\sum_{k=n}^{n+1}\left\|\mathbf{e}^{k}(x)\right\|_{L^2}^2-\frac{\sqrt{3}}{2}(b-a)\sum_{l=-M/2}^{M/2-1}\left(\left|\widehat{\mathbf{e}}_l^{n+1}\right|^2+\left|\widehat{\mathbf{e}}_l^{n}\right|^2\right)\\ =&\frac{2-\sqrt{3}}{2}(\left\|\mathbf{e}^{n+1}(x)\right\|_{L^2}^2+\left\|\mathbf{e}^{n}(x)\right\|_{L^2}^2).\end{aligned}\tag{6.26}$$

Multiplying (6.24) by $b-a$ and summing together for $l=-M/2,\ldots,M/2-1$, in view of the Bessel inequality, we obtain

$$\begin{aligned}\mathcal{E}^n-\mathcal{E}^{n-1}\lesssim&\tau(\left\|\mathbf{e}^{n+1}(x)\right\|_{L^2}^2+\left\|\mathbf{e}^{n}(x)\right\|_{L^2}^2+\left\|\mathbf{e}^{n-1}(x)\right\|_{L^2}^2)\\ &+\frac{1}{\tau}\|R^n(x)\|_{L^2}^2+\frac{1}{\tau}\|\xi^n(x)\|_{L^2}^2,\quad n\ge1.\end{aligned}\tag{6.27}$$

Summing (6.27) for $n=1,\ldots,m-1$, using (6.21) and (6.18), we derive

$$\mathcal{E}^{m-1}-\mathcal{E}^0\lesssim\tau\sum_{k=1}^{m}\left\|\mathbf{e}^{k}(x)\right\|_{L^2}^2+\frac{m\tau^5}{\varepsilon^8}+m\tau h^{2m_0},\quad 1\le m\le\frac{T}{\tau}.\tag{6.28}$$

Since $\mathbf{e}^0(x)=\mathbf{0}$ and $\mathcal{E}^{m-1}$ is bounded from below (6.26), we have for $1\le m\le\frac{T}{\tau}$,

$$\frac{2-\sqrt{3}}{2}(\|\mathbf{e}^{m}(x)\|_{L^2}^2+\|\mathbf{e}^{m-1}(x)\|_{L^2}^2)-\|\mathbf{e}^{1}(x)\|_{L^2}^2\lesssim\tau\sum_{k=1}^{m}\|\mathbf{e}^{k}(x)\|_{L^2}^2+\frac{m\tau^5}{\varepsilon^8}+m\tau h^{2m_0}.\tag{6.29}$$

Noticing $\|\mathbf{e}^1(x)\|_{L^2}\lesssim\frac{\tau^2}{\varepsilon^2}\lesssim\frac{\tau^2}{\varepsilon^4}$, the discrete Gronwall's inequality will imply that for sufficiently small τ,

$$\left\|\mathbf{e}^{m}(x)\right\|_{L^2}^2\lesssim h^{2m_0}+\frac{\tau^4}{\varepsilon^8},\quad 1\le m\le\frac{T}{\tau}.\tag{6.30}$$

Combining (6.14) and (6.30), we draw the conclusion (3.26). □

Appendix 3

Extensions of the sEWI-FS (3.16–3.17) and TSFP (4.4) in 2D and 3D

The sEWI-FS (3.16–3.17), sEWI-FP (3.18–3.19) and TSFP (4.4) can be easily extended to 2D and 3D with tensor grids by modifying the matrices Γ_l in (3.8) and $G(t,x)$ in (4.5) in the TSFP case. For the reader's convenience, we present the modifications of Γ_l in (3.8) and $G(t,x)$ in (4.5) in 2D and 3D as follows.

For the Dirac equation (1.21) *in 2D*, i.e. we take $d=2$ in (1.21). The problem is truncated on $\Omega=(a_1,b_1)\times(a_2,b_2)$ with mesh sizes $h_1=(b_1-a_1)/M_1$ and $h_2=(b_2-a_2)/M_2$ (M_1, M_2 two even positive integers) in the x- and y-direction, respectively. The wave function Φ is a two-component vector, and the matrix Γ_l in (3.8) will be replaced by

$$\Gamma_{jk}=\begin{pmatrix} 1 & \varepsilon\mu_j^{(1)}-i\varepsilon\mu_k^{(2)} \\ \varepsilon\mu_j^{(1)}+i\varepsilon\mu_k^{(2)} & -1 \end{pmatrix},\ \mu_j^{(1)}=\frac{2j\pi}{b_1-a_1},\ \mu_k^{(2)}=\frac{2k\pi}{b_2-a_2}, \tag{6.31}$$

where $-\frac{M_1}{2}\le j\le\frac{M_1}{2}-1$, $-\frac{M_2}{2}\le k\le\frac{M_2}{2}-1$, and the Schur decomposition $\Gamma_{jk}=Q_{jk}D_{jk}Q_{jk}^*$ is given as

$$Q_{jk}=\begin{pmatrix} \frac{1+\delta_{jk}}{\sqrt{2\delta_{jk}(1+\delta_{jk})}} & \frac{-\varepsilon\mu_j^{(1)}+i\varepsilon\mu_k^{(2)}}{\sqrt{2\delta_{jk}(1+\delta_{jk})}} \\ \frac{\varepsilon\mu_j^{(1)}+i\varepsilon\mu_k^{(2)}}{\sqrt{2\delta_{jk}(1+\delta_{jk})}} & \frac{1+\delta_{jk}}{\sqrt{2\delta_{jk}(1+\delta_{jk})}} \end{pmatrix},\quad D_{jk}=\begin{pmatrix}\delta_{jk} & 0\\ 0 & -\delta_{jk}\end{pmatrix}, \tag{6.32}$$

where

$$\delta_{jk}=\sqrt{1+\varepsilon^2(\mu_j^{(1)})^2+\varepsilon^2(\mu_k^{(2)})^2}. \tag{6.33}$$

The matrix $\int_{t_n}^{t_{n+1}}G(t,\mathbf{x})dt$ in (4.5) becomes $\int_{t_n}^{t_{n+1}}G(t,\mathbf{x})dt$ and the Schur decomposition $\int_{t_n}^{t_{n+1}}G(t,\mathbf{x})dt=P_{\mathbf{x}}\Lambda_{\mathbf{x}}P_{\mathbf{x}}^*$ with $V_{\mathbf{x}}^{(1)}=\int_{t_n}^{t_{n+1}}V(t,\mathbf{x})dt$, $A_{l,\mathbf{x}}^{(1)}=\int_{t_n}^{t_{n+1}}A_l(t,\mathbf{x})dt$ for $l=1,2$, $\lambda_{\mathbf{x}}^{(1)}=\sqrt{|A_{1,\mathbf{x}}^{(1)}|^2+|A_{2,\mathbf{x}}^{(1)}|^2}$, $\Lambda_{\mathbf{x}}=\mathrm{diag}(\Lambda_{\mathbf{x},+},\Lambda_{\mathbf{x},-})$, $\Lambda_{\mathbf{x},\pm}=V_{\mathbf{x}}^{(1)}\pm\lambda_{\mathbf{x}}^{(1)}$, and $P_{\mathbf{x}}=I_2$ if $\lambda_{\mathbf{x}}^{(1)}=0$ and otherwise

$$P_{\mathbf{x}}=\begin{pmatrix} \frac{1}{\sqrt{2}} & \frac{A_{1,\mathbf{x}}^{(1)}-iA_{2,\mathbf{x}}^{(1)}}{\sqrt{2}\lambda_{\mathbf{x}}^{(1)}} \\ -\frac{A_{1,\mathbf{x}}^{(1)}+iA_{2,\mathbf{x}}^{(1)}}{\sqrt{2}\lambda_{\mathbf{x}}^{(1)}} & \frac{1}{\sqrt{2}} \end{pmatrix}. \tag{6.34}$$

For the Dirac equation (1.9) *in 3D*, i.e. we take $d=3$ in (1.9). The problem is truncated on $\Omega=(a_1,b_1)\times(a_2,b_2)\times(a_3,b_3)$ with mesh sizes $h_1=(b_1-a_1)/M_1$, $h_2=(b_2-a_2)/M_2$ and $h_3=(b_3-a_3)/M_3$ (M_1, M_2, M_3 three even positive integers) in x-, y- and z-direction, respectively. The wave function Ψ is a four-component vector, and the matrix Γ_l in (3.8) will be replaced by Γ_{jkl} as:

$$\Gamma_{jkl}=\begin{pmatrix} 1 & 0 & \varepsilon\mu_l^{(3)} & \varepsilon\mu_j^{(1)}-i\varepsilon\mu_k^{(2)} \\ 0 & 1 & \varepsilon\mu_j^{(1)}+i\varepsilon\mu_k^{(2)} & -\varepsilon\mu_l^{(3)} \\ \varepsilon\mu_l^{(3)} & \varepsilon\mu_j^{(1)}-i\varepsilon\mu_k^{(2)} & -1 & 0 \\ \varepsilon\mu_j^{(1)}+i\varepsilon\mu_k^{(2)} & -\varepsilon\mu_l^{(3)} & 0 & -1 \end{pmatrix}, \tag{6.35}$$

where $-\frac{M_1}{2} \le j \le \frac{M_1}{2}-1, -\frac{M_2}{2} \le k \le \frac{M_2}{2}-1, -\frac{M_3}{2} \le l \le \frac{M_3}{2}-1$ and

$$\mu_j^{(1)} = \frac{2j\pi}{b_1-a_1}, \quad \mu_k^{(2)} = \frac{2k\pi}{b_2-a_2}, \quad \mu_l^{(3)} = \frac{2l\pi}{b_3-a_3}. \tag{6.36}$$

The eigenvalues of Γ_{jkl} are

$$\delta_{jkl}, \delta_{jkl}, -\delta_{jkl}, -\delta_{jkl}, \quad \text{with} \quad \delta_{jkl} = \sqrt{1+\varepsilon^2\left|\mu_j^{(1)}\right|^2+\varepsilon^2\left|\mu_k^{(2)}\right|^2+\varepsilon^2\left|\mu_l^{(3)}\right|^2}.$$

The corresponding eigenvectors are

$$\mathbf{v_{jkl}^{(1)}} = \begin{pmatrix} 1+\delta_{jkl} \\ 0 \\ \varepsilon\mu_l^{(3)} \\ \varepsilon\mu_j^{(1)}+i\varepsilon\mu_k^{(2)} \end{pmatrix}, \quad \mathbf{v_{jkl}^{(2)}} = \begin{pmatrix} 0 \\ 1+\delta_{jkl} \\ \varepsilon\mu_j^{(1)}-i\varepsilon\mu_k^{(2)} \\ -\varepsilon\mu_l^{(3)} \end{pmatrix},$$

and

$$\mathbf{v_{jkl}^{(3)}} = \begin{pmatrix} -\varepsilon\mu_l^{(3)} \\ -\varepsilon\mu_j^{(1)}-i\varepsilon\mu_k^{(2)} \\ 1+\delta_{jkl} \\ 0 \end{pmatrix}, \quad \mathbf{v_{jkl}^{(4)}} = \begin{pmatrix} -\varepsilon\mu_j^{(1)}+i\varepsilon\mu_k^{(2)} \\ \varepsilon\mu_l^{(3)} \\ 0 \\ 1+\delta_{jkl} \end{pmatrix}.$$

Then the Schur decomposition $\Gamma_{jkl} = Q_{jkl}D_{jkl}Q_{jkl}^*$ is given as

$$D_{jkl} = \mathrm{diag}(\delta_{jkl}, \delta_{jkl}, -\delta_{jkl}, -\delta_{jkl}), \quad Q_{jkl} = \frac{1}{\sqrt{2\delta_{jkl}(1+\delta_{jkl})}}\left(\mathbf{v_{jkl}^{(1)}}, \mathbf{v_{jkl}^{(2)}}, \mathbf{v_{jkl}^{(3)}}, \mathbf{v_{jkl}^{(4)}}\right).$$

The matrix $\int_{t_n}^{t_{n+1}} G(t,\mathbf{x})dt$ in (4.5) becomes $\int_{t_n}^{t_{n+1}} G(t,\mathbf{x})dt$ and the Schur decomposition $\int_{t_n}^{t_{n+1}} G(t,\mathbf{x})dt = P_{\mathbf{x}}\Lambda_{\mathbf{x}}P_{\mathbf{x}}^*$ with $V_{\mathbf{x}}^{(1)} = \int_{t_n}^{t_{n+1}} V(t,\mathbf{x})dt$, $A_{l,\mathbf{x}}^{(1)} = \int_{t_n}^{t_{n+1}} A_l(t,\mathbf{x})dt$ for $l = 1,2,3$, $\lambda_{\mathbf{x}}^{(1)} = \sqrt{|A_{1,\mathbf{x}}^{(1)}|^2+|A_{2,\mathbf{x}}^{(1)}|^2+|A_{3,\mathbf{x}}^{(1)}|^2}$, $\Lambda_{\mathbf{x}} = \mathrm{diag}(\Lambda_{\mathbf{x},+}, \Lambda_{\mathbf{x},+}, \Lambda_{\mathbf{x},-}, \Lambda_{\mathbf{x},-})$, $\Lambda_{\mathbf{x},\pm} = V_{\mathbf{x}}^{(1)} \pm \lambda_{\mathbf{x}}^{(1)}$, and $P_{\mathbf{x}} = I_4$ if $\lambda_{\mathbf{x}}^{(1)} = 0$ and otherwise $P_{\mathbf{x}} = (\mathbf{u}_{\mathbf{x}}^{(1)}, \mathbf{u}_{\mathbf{x}}^{(2)}, \mathbf{u}_{\mathbf{x}}^{(3)}, \mathbf{u}_{\mathbf{x}}^{(4)})$,

$$\mathbf{u}_{\mathbf{x}}^{(1)} = \begin{pmatrix} \frac{-A_{1,\mathbf{x}}^{(1)}+iA_{2,\mathbf{x}}^{(1)}}{\sqrt{2}\lambda_{\mathbf{x}}^{(1)}} \\ \frac{A_{3,\mathbf{x}}^{(1)}}{\sqrt{2}\lambda_{\mathbf{x}}^{(1)}} \\ 0 \\ \frac{1}{\sqrt{2}} \end{pmatrix}, \quad \mathbf{u}_{\mathbf{x}}^{(2)} = \begin{pmatrix} \frac{-A_{3,\mathbf{x}}^{(1)}}{\sqrt{2}\lambda_{\mathbf{x}}^{(1)}} \\ \frac{-A_{1,\mathbf{x}}^{(1)}-iA_{2,\mathbf{x}}^{(1)}}{\sqrt{2}\lambda_{\mathbf{x}}^{(1)}} \\ \frac{1}{\sqrt{2}} \\ 0 \end{pmatrix},$$

and

$$\mathbf{u}_{\mathbf{x}}^{(3)} = \begin{pmatrix} 0 \\ \frac{1}{\sqrt{2}} \\ \frac{A_{1,\mathbf{x}}^{(1)}-iA_{2,\mathbf{x}}^{(1)}}{\sqrt{2}\lambda_{\mathbf{x}}^{(1)}} \\ \frac{-A_{3,\mathbf{x}}}{\sqrt{2}\lambda_{\mathbf{x}}^{(1)}} \end{pmatrix}, \quad \mathbf{u}_{\mathbf{x}}^{(4)} = \begin{pmatrix} \frac{1}{\sqrt{2}} \\ 0 \\ \frac{A_{3,\mathbf{x}}^{(1)}}{\sqrt{2}\lambda_{\mathbf{x}}^{(1)}} \\ \frac{A_{1,\mathbf{x}}^{(1)}+iA_{2,\mathbf{x}}^{(1)}}{\sqrt{2}\lambda_{\mathbf{x}}^{(1)}} \end{pmatrix}.$$

For the Dirac equation (1.9) in 2D, we simply let $\mu_l^{(3)} = 0$, $A_3(t,\mathbf{x}) \equiv 0$ in the above 3D case; and for the Dirac equation (1.9) in 1D, we let $\mu_k^{(2)} = \mu_l^{(3)} = 0$, $A_2(t,\mathbf{x}) = A_3(t,\mathbf{x}) \equiv 0$ in the above 3D case. Then the sEWI-FP (3.18–3.19) and TSFP (4.4) can be designed accordingly for the Dirac equation (1.9) in 2D and 1D.

References

1. Abanin, D.A., Morozov, S.V., Ponomarenko, L.A., Gorbachev, R.V., Mayorov, A.S., Katsnelson, M.I., Watanabe, K., Taniguchi, T., Novoselov, K.S., Levito, L.S., Geim, A.K.: Giant nonlocality near the Dirac point in graphene. Science **332**, 328–330 (2011)
2. Abenda, S.: Solitary waves for the Maxwell–Dirac and Coulomb–Dirac models. Ann. Inst. Henri Poincaré Phys. Theor **68**, 229–244 (1998)
3. Ablowitz, M.J., Zhu, Y.: Nonlinear waves in shallow honeycomb lattices. SIAM J. Appl. Math. **72**, 240–260 (2012)
4. Anderson, C.D.: The positive electron. Phys. Rev. **43**, 491–498 (1933)
5. Antoine, X., Lorin, E., Sater, J., Fillion-Gourdeau, F., Bandrauk, A.D.: Absorbing boundary conditions for relativistic quantum mechanics equations. J. Comput. Phys. **277**, 268–304 (2014)
6. Archilla, B.G., Sanz-Serna, J.M., Skeel, R.D.: Long-time-step methods for oscillatory differential equations. SIAM J. Sci. Comput. **20**, 930–963 (1998)
7. Arnold, A., Steinrück, H.: The 'electromagnetic' Wigner equation for an electron with spin. ZAMP **40**, 793–815 (1989)
8. Bao, W., Cai, Y.: Mathematical theory and numerical methods for Bose–Einstein condensation. Kinet. Relat. Models **6**, 1–135 (2013)
9. Bao, W., Cai, Y.: Optimal error estmiates of finite difference methods for the Gross–Pitaevskii equation with angular momentum rotation. Math. Comput. **82**, 99–128 (2013)
10. Bao, W., Cai, Y.: Uniform and optimal error estimates of an exponential wave integrator sine pseudospectral method for the nonlinear Schrödinger equation with wave operator. SIAM J. Numer. Anal. **52**, 1103–1127 (2014)
11. Bao, W., Cai, Y., Zhao, X.: A uniformly accurate multiscale time integrator pseudospectral method for the Klein–Gordon equation in the nonrelativistic limit regime. SIAM J. Numer. Anal. **52**, 2488–2511 (2014)
12. Bao, W., Dong, X.: Analysis and comparison of numerical methods for the Klein–Gordon equation in the nonrelativistic limit regime. Numer. Math. **120**, 189–229 (2012)
13. Bao, W., Dong, X., Zhao, X.: An exponential wave integrator pseudospectral method for the Klein–Gordon–Zakharov system. SIAM J. Sci. Comput. **35**, A2903–A2927 (2013)
14. Bao, W., Dong, X., Zhao, X.: Uniformly correct multiscale time integrators for highly oscillatory second order differention equations. J. Math. Study **47**, 111–150 (2014)
15. Bao, W., Shi, J., Markowich, P.A.: On time-splitting spectral approximation for the Schrödinger equation in the semiclassical regime. J. Comput. Phys. **175**, 487–524 (2002)
16. Bao, W., Shi, J., Markowich, P.A.: Numerical study of time-splitting spectral discretizations of nonlinear Schrödinger equations in the semi-classical regimes. SIAM J. Sci. Comput. **25**, 27–64 (2003)
17. Bao, W., Li, X.: An efficient and stable numerical method for the Maxwell–Dirac system. J. Comput. Phys. **199**, 663–687 (2004)
18. Bechouche, P., Mauser, N., Poupaud, F.: (Semi)-nonrelativistic limits of the Dirac eqaution with external time-dependent electromagnetic field. Commun. Math. Phys. **197**, 405–425 (1998)
19. Bechouche, P., Mauser, N., Selberg, S.: On the asymptotic analysis of the Dirac–Maxwell system in the nonrelativistic limit. J. Hyper. Differ. Equat. **2**, 129–182 (2005)
20. Bolte, J., Keppeler, S.: A semiclassical approach to the Dirac equation. Ann. Phys. **274**, 125–162 (1999)
21. Booth, H.S., Legg, G., Jarvis, P.D.: Algebraic solution for the vector potential in the Dirac equation. J. Phys. A: Math. Gen. **34**, 5667–5677 (2001)
22. Bournaveas, N.: Local existence for the Maxwell–Dirac equations in three space dimensions. Commun. Part. Differ. Equ. **21**, 693–720 (1996)
23. Brinkman, D., Heitzinger, C., Markowich, P.A.: A convergent 2D finite-difference scheme for the Dirac–Poisson system and the simulation of graphene. J. Comput. Phys. **257**, 318–332 (2014)
24. Cirincione, R.J., Chernoff, P.R.: Dirac and Klein Gordon equations: convergence of solutions in the nonrelativistic limit. Commun. Math. Phys. **79**, 33–46 (1981)
25. Das, A.: General solutions of Maxwell–Dirac equations in 1 + 1 dimensional space-time and spatial confined solution. J. Math. Phys. **34**, 3986–3999 (1993)
26. Das, A., Kay, D.: A class of exact plane wave solutions of the Maxwell–Dirac equations. J. Math. Phys. **30**, 2280–2284 (1989)
27. Deuflhard, P.: A study of extrapolation methods based on multistep schemes without parasitic solutions. ZAMP **30**, 177–189 (1979)
28. Dirac, P.A.M.: The quantum theory of the electron. Proc. R. Soc. Lond. A **117**, 610–624 (1928)
29. Dirac, P.A.M.: A theory of electrons and protons. Proc. R. Soc. Lond. A **126**, 360–365 (1930)
30. Dirac, P.A.M.: Principles of Quantum Mechanics. Oxford University Press, London (1958)

31. Dolbeault, J., Esteban, M.J., Séré, E.: On the eigenvalues of operators with gaps: applications to Dirac operator. J. Funct. Anal. **174**, 208–226 (2000)
32. Esteban, M., Séré, E.: Existence and multiplicity of solutions for linear and nonlinear Dirac problems. Partial Differ. Equ. Appl. **12**, 107–112 (1997)
33. Esteban, M., Séré, E.: An overview on linear and nonlinear Dirac equations. Discrete Contin. Dyn. Syst. **8**, 381–397 (2002)
34. Faou, E., Schratz, K.: Asymptotic preserving schemes for the Klein–Gordon equation in the non-relativistic limit regime. Numer. Math. **126**, 441–469 (2014)
35. Fefferman, C.L., Weistein, M.I.: Honeycomb lattice potentials and Dirac points. J. Am. Math. Soc. **25**, 1169–1220 (2012)
36. Fefferman, C.L., Weistein, M.I.: Wave packets in honeycomb structures and two-dimensional Dirac equations. Commun. Math. Phys. **326**, 251–286 (2014)
37. Ferreira, A., Gomes, J.V., Nilsson, J., Mucciolo, E.R., Peres, N.M.R., Catro Neto, A.H.: Unified description of the dc-conductivity of monolayer and bilayer graphene at finite densities based on resonant scatterers. Phys. Rev. B **83**, 165402 (2011)
38. Fillion-Gourdeau, F., Lorin, E., Bandrauk, A.D.: Resonantly enhanced pair production in a simple diatomic model. Phys. Rev. Lett. **110**, 013002 (2013)
39. Fillion-Gourdeau, F., Lorin, E., Bandrauk, A.D.: A split-step numerical method for the time-dependent Dirac equation in 3-D axisymmetric geometry. J. Comput. Phys. **272**, 559–587 (2014)
40. Foldy, L.L., Wouthuysen, S.A.: On the Dirac theory of spin 1/2 particles and its nonrelavistic limit. Phys. Rev. **78**, 29–36 (1950)
41. Fushchich, W.I., Shtelen, W.M.: On some exact solutions of the nonlinear Dirac equation. J. Phys. A: Math. Gen. **16**, 271–277 (1983)
42. Gautschi, W.: Numerical integration of ordinary differential equations based on trigonometric polynomials. Numer. Math. **3**, 381–397 (1961)
43. Gérad, P., Markowich, P.A., Mauser, N.J., Poupaud, F.: Homogenization limits and Wigner transforms. Commun. Pure Appl. Math. **50**, 321–377 (1997)
44. Gesztesy, F., Grosse, H., Thaller, B.: A rigorious approach to relativistic corrections of bound state energies for spin-1/2 particles. Ann. Inst. Henri Poincaré Phys. Theor **40**, 159–174 (1984)
45. Gosse, L.: A well-balanced and asymptotic-preserving scheme for the one-dimensional linear Dirac equation. BIT Numer. Math. **55**, 433–458 (2015)
46. Grigore, D.R., Nenciu, G., Purice, R.: On the nonrelativistic limits of the Dirac Hamiltonian. Ann. Inst. Henri Poincaré Phys. Theor **51**, 231–263 (1989)
47. Gross, L.: The Cauchy problem for the coupled Maxwell and Dirac equations. Commun. Pure Appl. Math. **19**, 1–15 (1966)
48. Hammer, R., Pötz, W., Arnold, A.: Single-cone real-space finite difference scheme for the time-dependent Dirac equation. J. Comput. Phys. **265**, 50–70 (2014)
49. Hammer, R., Pötz, W., Arnold, A.: A dispersion and norm preserving finite difference scheme with transparent boundary conditions for the Dirac equation in (1 + 1)D. J. Comput. Phys. **256**, 728–747 (2014)
50. Hairer, E., Lubich, C., Wanner, G.: Geometric Numerical Integration. Springer, Berlin (2002)
51. Hochbruck, M., Lubich, C.: A Gautschi-type method for oscillatory second-order differential equations. Numer. Math. **83**, 402–426 (1999)
52. Hochbruck, M., Ostermann, A.: Exponential integrators. Acta Numer. **19**, 209–286 (2000)
53. Huang, Z., Jin, S., Markowich, P.A., Sparber, C., Zheng, C.: A time-splitting spectral scheme for the Maxwell–Dirac system. J. Comput. Phys. **208**, 761–789 (2005)
54. Hunziker, W.: On the nonrelativistic limit of the Dirac theory. Commun. Math. Phys. **40**, 215–222 (1975)
55. Iserles, A.: A First Course in the Numerical Analysis of Differential Equations. Cambridge University Press, Cambridge (2008)
56. Iserles, A., Norsett, S.P.: From high oscillation to rapid approximation I: modified Fourier expansions. IMA J. Numer. Anal. **28**, 862–887 (2008)
57. Kammerer, C.F.: Semi-classical analysis of a Dirac equaiton without adiabatic decoupling. Monatsh. Math. **142**, 281–313 (2004)
58. Lubich, C.: On splitting methods for Schrödinger–Poisson and cubic nonlinear Schrödinger equations. Math. Comput. **77**, 2141–2153 (2008)
59. Masmoudi, N., Mauser, N.J.: The selfconsistent Pauli equaiton. Monatsh. Math. **132**, 19–24 (2001)
60. Mauser, N.J.: Rigorous derivation of the Pauli equation with time-dependent electromagnetic field. VLSI Design **9**, 415–426 (1999)
61. Najman, B.: The nonrelativistic limit of the nonlinear Dirac equation. Ann. Inst. Henri Poincaré **9**, 3–12 (1992)

62. Neto, A.H.C., Guinea, F., Peres, N.M.R., Novoselov, K.S., Geim, A.K.: The electronic properties of the graphene. Rev. Mod. Phys. **81**, 109–162 (2009)
63. Novoselov, K.S., Geim, A.K., Morozov, S.V., Jiang, D., Katsnelson, M.I., Grigorieva, I.V., Dubonos, S.V., Firsov, A.A.: Two-dimensional gas of massless Dirac fermions in graphene. Nature **438**, 197–200 (2005)
64. Novoselov, K.S., Geim, A.K., Morozov, S.V., Jiang, D., Zhang, Y., Dubonos, S.V., Grigorieva, I.V., Firsov, A.A.: Electric filed effect in atomically thin carbon films. Science **306**, 666–669 (2004)
65. Novoselov, K.S., Jiang, Z., Zhang, Y., Morozov, S.V., Stormer, H.L., Zeitler, U., Maan, J.C., Boebinger, G.S., Kim, P., Geim, A.K.: Room-temperature quantum Hall effect in graphene. Science **315**, 1379 (2007)
66. Nraun, J.W., Su, Q., Grobe, R.: Numerical approach to solve the time-dependent Dirac equation. Phys. Rev. A **59**, 604–612 (1999)
67. Schedin, F., Geim, A., Morozov, S., Hill, E., Blake, P., Katsnelson, M., Novoselov, K.: Detection of individual gas molecules absorbed on graphene. Nat. Mater. **6**, 652–655 (2007)
68. Schoene, A.Y.: On the nonrelativistic limits of the Klein–Gordon and Dirac equations. J. Math. Anal. Appl. **71**, 36–74 (1979)
69. Shebalin, J.V.: Numerical solution of the coupled Dirac and Maxwell equations. Phys. Lett. A **226**, 1–6 (1997)
70. Shen, J., Tang, T.: Spectral and High-Order Methods with Applications. Science Press, Beijing (2006)
71. Smith, G.D.: Numerical Solution of Partial Differential Equations: Finite Difference Methods. Clarendon Press, Oxford (1985)
72. Spohn, H.: Semiclassical limit of the Dirac equaiton and spin precession. Ann. Phys. **282**, 420–431 (2000)
73. Strang, G.: On the construction and comparision of difference schemes. SIAM J. Numer. Anal. **5**, 505–517 (1968)
74. Thaller, B.: The Dirac Equation. Springer, New York (1992)
75. Veselic, K.: Perturbation of pseudoresolvents and analyticity in $1/c$ ofrelativistic quantum mechanics. Commun. Math. Phys. **22**, 27–43 (1971)
76. White, G.B.: Splitting of the Dirac operator in the nonrelativistic limit. Ann. Inst. Henri Poincaré **53**, 109–121 (1990)
77. Wu, H., Huang, Z., Jin, S., Yin, D.: Gaussian beam methods for the Dirac equation in the semi-classical regime. Commun. Math. Sci. **10**, 1301–1315 (2012)